https://doi.org/10.5194/acp-2022-842
Preprint. Discussion started: 11 January 2023

Atmospheric Chemistry and Physics Discussions

A one-year ACSM source analysis of organic aerosol particle contributions from anthropogenic sources after long-range transport at the TROPOS research station Melpitz

Samira Atabakhsh[1], Laurent Poulain[1], Gang Chen[2,3], Francesco Canonaco[2,4], André Prévôt[2], Mira Pöhlker[1], Alfred Wiedensohler[1], Hartmut Herrmann[1]

[1]Leibniz Institute for Tropospheric Research, Leipzig, 04318, Germany
[2]Laboratory of Atmospheric Chemistry, Paul Scherrer Institute, Villigen, Aargau, 5232, Switzerland
[3]MRC Centre for Environment and Health, Environmental Research Group, Imperial College London, London, W12 0BZ, U.K.
[4]Datalystica Ltd., Park innovAARE, Villigen, Aargau, 5234,Switzerland

Correspondence to: Hartmut Herrmann (herrmann@tropos.de)

Abstract

Atmospheric aerosol particles are a complex combination of primary emitted sources (biogenic and anthropogenic) and secondary aerosol resulting from the aging processes such as condensation, coagulation, and cloud processing. To better understand their sources, investigations have been focused on source identification in urban areas in the past, while rural background stations are normally less impacted by surrounding anthropogenic sources. Therefore, they are predisposed for studying the impact of long-range transport of anthropogenic aerosols. Moreover, long-term measurements can help to study the potential temporal changes in the sources. Here, the chemical composition and organic aerosol sources of submicron aerosol particles were investigated at the Central European rural-background research station, Melpitz, using a one yearlong dataset determined by an aerosol chemical speciation monitor (ACSM) and a multi-angle absorption photometer (MAAP) from September 2016 to August 2017. Melpitz represents due to its location the Central European aerosol. It is an ideal location to investigate the impact of long-range transport, since the location is influenced by less polluted air masses from westerly directions and more polluted continental air masses from Eastern Europe. The organic aerosol (OA) dominated the submicron particle mass concentration and showed strong seasonal variability ranging from 39 % (in winter) to 58 % (in summer). It was followed by sulphate (15 % and 20 %) and nitrate (24 % and 11 %). The OA source identification was performed using rolling positive matrix factorisation (PMF) approach to account for the potential temporal changes in the source profile (SoFi Pro). It was possible to split OA into five-factors with a distinct temporal variability and mass spectral signature. Three were associated to anthropogenic primary OA (POA) sources: hydrocarbon-like OA (HOA, 5.2 % of OA mass in winter and 6.8 % in summer), biomass burning OA (BBOA, 10.6 % and 6.1 %) and coal combustion OA (CCOA, 23 % and 8.7 %). Another two are secondary/processed oxygenated OA (OOA) sources: less-oxidized OOA (LO-OOA, 28.4 % and 36.7 %) and more-oxidized OOA (MO-OOA, 32.8 % and 41.8 %). Since equivalent black carbon (eBC) was clearly associated with the identified POA

https://doi.org/10.5194/acp-2022-842
Preprint. Discussion started: 11 January 2023

Atmospheric Chemistry and Physics Discussions

factors (sum of HOA, BBOA and CCOA, R^2= 0. 87), eBC's contribution to each of the POA factors was achieved using a multi-linear regression model. Consequently, CCOA represented the main anthropogenic sources of carbonaceous aerosol (sum of OA and eBC) not only during winter (56 % of POA in winter) but also in summer (13 % of POA in summer), followed by BBOA (29 % and 69 % of POA in winter and summer, respectively) and HOA (15 % and 18 % of POA in winter and summer, respectively). A seasonal air mass cluster analysis was used to understand the geographical origins of the different aerosol types and show that during both winter and summer time, PM_1 (PM with aerodynamic diameter smaller than 1µm) air masses with eastern influence was always associated with the highest mass concentration and the highest coal combustion fraction. Since during winter time, CCOA is a combination of domestic heating and power plants emissions, the summer contribution of CCOA emphasises the critical importance of coal power plants emissions to rural background aerosols and its impact on air quality, through long-range transportation.

1 Introduction

Human health effects of air pollution from particulate matter (PM) are well known, and efforts are being made across the world (*WHO, Expert Consultation*, 2019) to minimize both long-term exposure to harmful levels and air pollution peaks. Throughout all the PMs, the submicronic particles known as PM_1 (particles with an aerodynamic diameter less than 1 µm), not only have a negative impact on human health (Daellenbach et al., 2020) but also have a significant effect on visibility (Shi et al., 2014) and climate (Shrivastava et al., 2017). Since the most numerous component of the atmospheric PM is the organic aerosol (OA) (Jimenez et al., 2009; Chen et al., 2022), contributions to OA and explanations of its chemical and physical characteristics remain challenging, whereas the large variety of OA can be attributed to primary emissions by various sources in different seasons, as well as different reactions to atmospheric dynamics and complicated chemical mechanisms depending on meteorological parameters and geographical locations.

In order to evaluate and recognize the sources of OA emission, aerosol mass spectrometers (AMS, Jayne et al., 2000) and aerosol chemical speciation monitors (ACSM) (Ng et al., 2011; Fröhlich et al., 2013) are widely deployed worldwide (Chen et al., 2022; Bressi et al., 2021; Fröhlich et al., 2015). AMS is commonly limited to short time periods due to the high maintenance of the AMS measurements and their high operating costs. As a result, only a few studies run AMS continuously (e.g., see Kumar et al., 2022 and O'Dowd et al., 2014). However, there was still a strong need for such a long-term analysis. ACSM is designated for long-term monitoring purposes due to its robustness and much less labour-intense compared to AMS. Therefore, the deployment of ACSM allows us to look at the long-term (more than one year) temporal changes and/or seasonal variability of OA sources.

Regarding the identification of OA sources, source apportionment analysis using positive matrix factorisation algorithm (PMF, Paatero and Tappert, 1994) was intensively used over the past two decades on both AMS and ACSM measurements (e.g. see Crippa et al., 2014; Poulain et al., 2020). However, this algorithm faced two main limitations when used during a long time period: firstly, the factor profiles are static over the analyzing period (Paatero, 1997); and secondly, rotational ambiguity which

https://doi.org/10.5194/acp-2022-842
Preprint. Discussion started: 11 January 2023

Atmospheric Chemistry and Physics Discussions

provides non-unique solutions. To solve these issues, a multilinear engine (ME-2, Paatero, 1999) has been implemented in the PMF analysis, which allows use of a priori knowledge to constrain the model to environmentally reasonable solutions (e.g., Lanz et al., 2008; Canonaco et al., 2013; Crippa et al., 2014). To consider the temporal variation of the factor profiles, a rolling approach was suggested (Parworth et al., 2015; Canonaco et al., 2020). The rolling strategy involves advancing a smaller PMF window (i.e., 14 days) and moving/rolling it over the whole dataset to catch the temporal changes of the source profiles with a 1-day step.

Although several studies in Europe have already conducted source apportionment analyses of one year or more, most of them were associated with urban or suburban environments (e.g., for urban studies: Stavroulas et al., 2019; Vlachou et al., 2019; Huang et al., 2019; Qi et al., 2020; and for suburban studies: Katsanos et al., 2019; Y. Zhang et al., 2019), and only a few of them were studied in rural-background sites (Schlag et al., 2016; Crippa et al., 2014; Vlachou et al., 2018; Paglione et al., 2020; Dudoitis et al., 2016; Heikkinen et al., 2020; Chen et al., 2021; and Chen et al., 2022), although the rural-background sites represent the major advantage to be able to study the impact of long-range transport of anthropogenic emissions and their changes over a long time period. The Leibniz Institute for Tropospheric Research (TROPOS) Central European observatory Melpitz has been continuously measuring aerosol chemical composition for 30 years. The station is a unique place in Europe, sitting at the border between marine-influenced Western Europe and continental Eastern Europe. A direct consequence is that the aerosol chemical composition and mass concentration strongly depend on the air mass origins, showing less polluted air masses coming from the West and more polluted air masses from the East (Birmili et al., 2001; Spindler et al., 2010). However, only a few studies were done on the source identification of the aerosol reaching the station by covering short time periods mostly during winter (van Pinxteren et al., 2016, 2023).

The current study comprehensively investigates the PM_1 aerosol particle chemical compositions and the various OA sources for Melpitz based on ACSM and multi-angle absorption photometer (MAAP) measurements from September 2016 to August 2017, using the most advanced rolling PMF with ME-2 implemented in the SoFi Pro package (Datalystica Ltd., Villigen, Switzerland) (Parworth et al., 2015; Canonaco et al., 2013; Canonaco et al., 2020). Moreover, a multi-linear regression model was used to estimate the contribution of equivalent black carbon (eBC) to the various PMF factors. Meanwhile, the influence of air mass origin was investigated to identify the emission area of the different PM_1 sources.

2 Methodology

2.1 Sampling site

The atmospheric aerosol measurements were carried out at the TROPOS research station Melpitz (51.54° N, 12.93° E, 86 m a.s.l.), located approximately 50 km northeast of Leipzig, Germany. The station itself is mainly encircled by agronomical pastures and forests within a rural area, which is why the station is recognized as a rural-background station (Spindler et al., 2013). Since 1992, the station has been monitoring the influence of atmospheric long-range transport on background air quality of Central European (e.g. Spindler et al., 2012 2013). The Melpitz station is part of EMEP (European Monitoring and

https://doi.org/10.5194/acp-2022-842
Preprint. Discussion started: 11 January 2023


Atmospheric Chemistry and Physics Discussions

Evaluation Programme; Level 3 station, Aas et al., 2012), ACTRIS (Aerosol, Clouds and Trace gases Research Infrastructure), GAW (Global Atmosphere Watch of the World Meteorological Organization), and GUAN (German Ultrafine Aerosol Network, Birmili et al., 2009, 2015, 2016). For a general description of the chemical and physical aerosol characterization analysis techniques, check e.g. Spindler et al., (2004, 2010, 2012, 2013); and Poulain et al., (2011, 2014, 2020).

2.2 ACSM

The chemical compositions and mass loadings of non-refractory PM_1 (NR-PM_1: organic, sulphate, nitrate, ammonium, and chloride) with a 30-minute time resolution were measured by an Aerodyne quadrupole ACSM. The ACSM sampling technique and operational information were previously detailed by Ng et al., (2011).

Briefly, after PM_1 transmits across a 100 µm critical orifice, the aerosols are centralized into a slender beam in an aerodynamic lens (Liu et al., 2007). Non-refractory particulate material that evaporates at the oven temperature (generally 600°C) is recorded and chemically determined using electron impact quadrupole mass spectrometry at 70 eV (Ng et al 2011). The ions are then detected using a quadrupole residual gas analyser (RGA, Pfeiffer Vacuum Prisma Plus). The ACSM takes 30 second samples of both ambient and particle-free air. The difference in these measurements identifies the aerosol mass spectrum. To change the signal spectra into organic or inorganic species concentrations, the fragmentation table (Allan et al., 2004), the ion transmission correction, and the Response Factor (RF) are applied. To improve the particle loss as a result of bouncing off the vaporizer, the ACSM data were processed according to manufacturer guidelines with using a composition dependent collection efficiency (CDCE) correction relying on the algorithms suggested by Middlebrook et al. (2012). Calibrations of Ionization Efficiency (IE) and Relative Ion Efficiency (RIE) were performed using a 350 nm monodispersed ammonium nitrate and ammonium sulphate (Ng et al., 2011). The final mean value for IE was $4.93(\pm1.45) \times 10^{-11}$ and the mean values for RIEs for ammonium and sulphate respectively were 6.48±1.26, and 0.68±0.13. Details on the QA/QC for this dataset can be found in Poulain, et al., (2020).

2.3 Additional measurements

In parallel to the ACSM, a MAAP was used to measure the mass concentrations of equivalent black carbon (eBC) (model 5012 Thermo Scientific; Petzold and Schönlinner, 2004). Conversion of the eBC mass concentration from the PM_{10} inlet to the ACSM PM_1 cut-off was made by applying a correction factor of 0.9 following Poulain et al (2011). Furthermore, a dual mobility particle size spectrometer (TROPOS-type T-MPSS; Birmili et al., 1999) was used to measure the PNSD from 3 to 800 nm (mobility diameter, d mob) at ambient and 300°C temperatures (Wehner et al., 2002). The MAAP was situated in the same laboratory container as the ACSM and these instruments sampled the same PM_{10} inlet after a dryer, and the sampled air distribution among the instruments was equally assured by an isokinetic splitter (Poulain et al., 2020).

In addition to the online measurements, high-volume samplers (DIGITEL DHA-80, Digitel Elektronik AG, Hegnau, Switzerland) were utilized to capture daily $PM_{2.5}$ samples on a quartz filter (for 24 hours from midnight to midnight). For more

https://doi.org/10.5194/acp-2022-842
Preprint. Discussion started: 11 January 2023


Atmospheric Chemistry and Physics Discussions

details on the sample preparation and evaluation methods, see Spindler et al., (2013). Levoglucosan as a tracer for wood burning combustion was measured following Iinuma et al., (2009) using high performance anion exchange chromatography coupled with an electrochemical detector (HPAEC-PAD) that was used for the analysis of anhydro-monosaccharides (Iinuma et al., 2009).

Trace gas measurements were also carried out. Ozone was determined by a U.V. Photometric gas analyser mode 49C (Thermo Scientific, UK), SO_2 by an APSA-360A (Horiba, Kyoto, Japan), and NO and NO_2 using a customized Trace Level NOx Analysis Model 42i-TL (Thermo Scientific) equipped with a blue light converter. Standard meteorological parameters (temperature, relative humidity, solar radiation, precipitation, wind direction, and wind speed) were regularly measured.

2.4 Rolling PMF (ME-2) source apportionment of OA

This work conducted the most advanced source apportionment analysis following a standardized protocol developed by Chen et al., (2022). The PMF method was used to allocate the source of the OA (Paatero and Tappert, 1994) through the Source Finder professional (SoFi Pro, Canonaco et al., 2021) software package (Datalystica Ltd., Villigen, Switzerland), within the Igor Pro software environment (Wavemetrics, Inc., Lake Oswego, OR, USA). Two matrices of factor profiles *F* and factor contributions *G*, defined the dataset *X*, and the matrix *E* named the residual matrix is the fraction which cannot be described by the model. Time series and the chemical fingerprint of sources respectively have been represented by F_{kj} and G_{ik}, respectively. The dimension of F_{kj} and G_{ik} are based on the order *p*, which is the number of factors selected to represent the data which is defined by the user:

$$X_{ij} = \sum_{k=1}^{p} G_{ik} \times F_{kj} + E_{ij} \quad (1)$$

In this study, since the measurement covers a period of 12 months (full four seasons), four separate PMF inputs were prepared. Unconstrained PMF was applied with 4 to 6 factors runs for all the seasons; throughout the pre-result and while referring to previous studies (Crippa et al., 2014 and van Pinxteren et al., 2016) primary factors were separated as hydrocarbon-like OA (HOA), biomass burning OA (BBOA) and coal combustion OA (CCOA). However, unconstrained PMF did not result to separate the primary factor profiles. Introducing constraints based on prior knowledge is an efficient strategy for avoiding the mixing of primary factors (Canonaco et al., 2013; Crippa et al., 2014). For this reason, the multilinear engine (ME-2) algorithm (Paatero, 1999) enables the incorporation of time series and factor profiles constraints in form of the *a*-value approach. In dealing with a profile constraint, the *a*-value specifies the variety of a factor that can deviate from the anchor profile during the PMF iteration:

$$f_{j,solution} = f_j \pm a \,.\, f_j \quad (2)$$

https://doi.org/10.5194/acp-2022-842
Preprint. Discussion started: 11 January 2023

Atmospheric Chemistry and Physics Discussions

The constraints applied through ME-2 for HOA and BBOA sources used the anchor profile of Crippa et al., (2014), and Ng et al., (2010), respectively. The anchor profile used for CCOA was generated from our own winter data during this work (SI, 1.1). For each of the four seasons, primary profiles were subject to a sensitivity analysis with *a-values* ranging from 0-0.4 for HOA and BBOA, 0-0.5 for CCOA, and steps of 0.1 to choose the best *a-value* combination for these three factors.

In the PMF approach, there is the intrinsic property of static factor profiles during the period of PMF analysis. Even though for short-term measurements (like one/two season/s) this might be a sensible estimation, long-term observations as are typical for current ACSM study (one year and more), are expected to be subject to evolving factor profiles based on seasonality. To consider the temporal changes, the rolling PMF window method was developed (Canonaco et al., 2021b; Parworth et al., 2015). This technique is applied to a small window, which is slowly extended throughout the whole dataset. Based on the dataset, the user determines the width of the PMF window, the shift parameter, and the number of PMF repeats per window; for the current work, we set 14-day windows, 1-day shifts, and 100 repeats per window.

In addition, this rolling PMF analysis was coupled with the bootstrap re-sampling approach (*Bootstrap Methods: Another Look at the Jackknife on JSTOR*, 1979), which can randomly select a part of the original matrix and repeat a part of the rows to generate a new same-sized matrix to test the stability of solutions and to estimate the statistical error. Overall, we have combined rolling PMF with ME-2 and bootstrap to conduct the source apportionment investigation, and more information on this new approach was described in Canonaco et al., (2020). This approach for a yearlong dataset generates an enormous amount of PMF runs (N= 35800) and not all of the solutions are environmentally reasonable. Since it is practically impossible to manually inspect all PMF runs, the criterial-base selection was introduced in SoFi Pro to automatically and objectively select environmentally reasonable PMF solutions (Canonaco et al., 2020). Finally, the resulting factors were interpreted as HOA, BBOA, CCOA and two oxidized OA (OOA) factors named less-oxygenated OOA (LO-OOA) and more oxygenated OOA (MO-OOA). The steps and setups utilized in the evaluation of this dataset are detailed in the supplement (Sect. 1).

2.5 Air mass trajectory analysis

Non-parametric wind regressions (NWR) were used to approximate the OA source concentrations at a given wind direction and speed (Henry et al., 2009). The NOAA HYbrid Single-Particle Lagrangian Integrated Trajectory (HYSPLIT-4) model was used to analyse 96 h backward trajectories at 500 m above the model ground of the sampling place (Draxler and Hess, 2004). The trajectory results were used for two independent but complementary analyses to better depict the emission area of the aerosol: by identifying the potential aerosol sources area and by clustering the trajectories.

A cluster analysis of the different trajectories was performed. The synoptic-scale air mass condition, together with geographical location and paths, is a crucial driver of local pollutant concentrations (e.g. Sun et al., 2020; Ma et al., 2014). Local particle mass concentrations and meteorological conditions can play a significant role and be associated with specific air mass trajectories. In addition, the trajectories of the air mass can influence aerosol compositions. For example, the stability of the atmosphere is also meaningful since it influences both the vertical dilution of pollutants and the overall particle mass

https://doi.org/10.5194/acp-2022-842
Preprint. Discussion started: 11 January 2023


Atmospheric Chemistry and Physics Discussions

concentration. Therefore, the effects of inter-annual variations in air mass conditions and the stability of atmosphere on observed patterns were inspected using a self-developed back-trajectory cluster method (BCLM), concerning air mass backward trajectories, pseudo-potential temperature profiles, PM_{10} mass concentration profiles over Melpitz, and seasons (Birmili et al., 2010; Ma et al., 2014). Descriptive analysis, cluster processing, and data processes and products are all described in detail by Sun et al., (2020) and Ma et al., (2014).

3 Results

3.1 PM_1 chemical composition

In this work, we investigate one-year long measurements of PM_1 for Melpitz, Germany. All the data is presented in UTC, during the winter and summer, the time zone is one and two hours behind local time, respectively. Yearly time series, seasonal variation, and diurnal cycles of aerosol particle chemical compositions including mass concentration and mass fraction, as measured by ACSM and MAAP, are shown in figures 1, 2, and 3, respectively. Over the entire period, the chemical composition of PM_1 was basically made up of organic aerosol (46 % of the total mass; Fig. 1c), sulphate (16 %), nitrate (21 %), ammonium (11 %), eBC (6 %), and chloride (close to 0 %). However, a mean mass concentration of 10.47 µg/m^3 (Fig. 1) was obtained with an obvious seasonal trend which detected the highest total mass concentrations (15.95 µg/m^3) during the winter time and lowest mass concentration during the summer time; 6.24 µg/m^3 (Fig. 1a and Fig. 2a). Compared to previous AMS measurements of Poulain et al., (2011) at the same station, a similar seasonal trend was observed in the period 2008/2009, while the absolute masses differed (Table. S1), which is at least partially related to the inter-annual changes of the meteorological conditions. Fig. S2 presents the coming high polluted air masses for total PM_1 to the measurement site in the current study; the polluted Eastern Europe flow with high mass concentration and south-west with low mass concentration was more clearly found in winter time rather than in other seasons, which will be comprehensively discussed in the Sect. 3.4.
In comparison with other ACSM/AMS rural-background stations in Europe which can be divided into three parts Northern Europe (NE), Southern Europe (SE), and Mid-latitude Europe (ME) (Bressi et al., 2021), the annual PM_1 mean mass concentration measured at Melpitz is similar to the value obtained at other ME stations, such as Magadino 10.1 µg/m^3, Kosetice 8.5 µg/m^3 (Chen et al., 2022), 9.1 µg/m^3 on average of PM_1 mean mass concentration of 6 stations (Ispra, Melpitz, Magadino, Cabauw, Sirta and Hohenpeissenberg, Bressi et al., 2021).

3.1.1 Inorganic

The seasonality of the inorganic species can be associated with their variations in emissions and/or the changes in their chemical atmospheric processes. Throughout the year, the mass concentration and their respective contribution to the total PM_1 mass of nitrate, ammonium, and chloride increased from a minimum value in summer (11 %, 7 %, and 0 %, respectively; Fig. 2b) and reached a maximum value in winter (24 %, 12 %, and 1 %, respectively; Fig. 2b). Sulphate showed a slightly different behavior. Although the contribution of sulphate to the total PM_1 decreased slightly from summer (20 %) to winter

https://doi.org/10.5194/acp-2022-842
Preprint. Discussion started: 11 January 2023


Atmospheric Chemistry and Physics Discussions

(15 %), its mass concentration remained higher in winter compared to summer (2.38 µg/m^3 and 1.23 µg/m^3, respectively; Table. 1). The enhancement is not as drastic as other inorganic species since sulphate is least volatile, therefore, more fraction of sulphate stayed in particle phase even in summer. Moreover, with enhanced irradiations in summer, sulphate formation from photochemistry could be enhanced as well. This result is consistent with the mean PM_1 mass concentration measured by AMS for the three periods during fall (16. September.2008 to 03. November.2008), winter (24. February.2009 to 25. March.2009), and summer (23. May.2009 to 09. June.2009) campaigns reported by Poulain et al., (2011). The diurnal cycles of sulphate (Fig. 3) showed a different daily pattern in warm and cold seasons. In summer, sulphate mass concentration increased during the day and reached its maximum level at 12:00 UTC (Fig. 3) due to sulphur dioxide photochemical oxidation processes in the atmosphere, which also presented the highest mass concentration during the day, along with maximum temperature and sun radiation in summer time (Fig. S3). Furthermore, the wind rose analysis showed a high mass concentration of sulphate at low wind speed (Fig S3). Although locally formed emissions of sulphate (Fig. S2) can explain this peak during the day in summer, this photochemical process is not the only source of sulphate. It especially cannot explain the highest mass concentrations during the winter time with almost no diurnal variation (Fig. 3). For winter, the emission of domestic heating processes, which could be enhanced in the atmospheric boundary layer (Stieger et al., 2018), along with the long range transported emissions, which came from north-east toward the measurement site (Fig. S2), and also high ammonium nitrate due to partitioning according to temperature, explain the high mass concentration but the low relative contribution of sulphate.

Nitrate is mostly found in the form of ammonium-nitrate (NH_4NO_3), which is reliant on the gas phase precursor concentrations, temperature, humidity, and aerosol chemical composition (Poulain et al. 2011; Stieger et al., 2018). Both nitrate and ammonium showed a minimum mass fraction and mass concentration in summer (11 %, 0.68 µg/m^3, 7 %, 0.43 µg/m^3, respectively; Fig. 2), an increasing trend toward the cold months and reached their maximum mass fraction and mass concentration in winter time (nitrate 24 %, 3.87 µg/m^3, ammonium 12 %, 2 µg/m^3, respectively; Fig. 2). The diurnal cycles of nitrate and ammonium (Fig. 3) showed a relatively similar daily pattern in all seasons, which means the highest values were reached in the morning, due to the beginning of vertical mixing and a reduction in the afternoon followed by an increase during the night, reflecting their night time production during every season. The volatile behaviour of ammonium-nitrate strongly affects its temporal variation during warm days leading to the formation of the gaseous nitric acid and ammonia compounds at higher temperatures and low humidity (Fig. S3, and S3). In winter, ammonium-nitrate remains mainly in the particle phase (Seinfeld and Pandis, 2006) and, like sulphate, arrived at the measurement site due to the long-range transported emissions which not only came from the north-eastern but also south-western flow, describing higher mass concentrations for nitrate and ammonium (Fig. S2). High values of nitrate and ammonium in spring time are linked to agronomical fertilization (Stieger et al., 2018). These seasonal contribution results for both, nitrate and ammonium, are consistent with the previous AMS study (Poulain et al., 2011), with minimum fraction to the total AMS-PM_1 during summer (nitrate 5 % and ammonium 8 %; Table. S1), and maximum fraction during winter time (nitrate 34 % and ammonium 17 %; Table. S1). However, it is known that a

https://doi.org/10.5194/acp-2022-842
Preprint. Discussion started: 11 January 2023


Atmospheric Chemistry and Physics Discussions

fraction of the nitrate signal can be attributed to nitrogen containing organic species (Kiendler-Scharr et al., 2016), which can affect the overall nitrate mass concentration (Poulain et al., 2020).

Although chloride had the lowest annual mass concentration (0.05 µg/m^3) compared to all other PM_1 chemical components (Table. 1), it showed the highest mass concentration and mass fraction in winter (0.11 µg/m^3, 1 %, respectively; Fig. 2a&b; Table. 1) compared to the other seasons; as seen in the previous AMS study of Poulain et al., (2011) (2 %, Table. S1). It could be related to the surrounding and transported emissions which were high for air masses from north-easterly and south-westerly directions (Fig. S2). In a multi-year analysis of the hourly PM_{10} chloride mass concentration measurements using a MARGA, Stieger et al., (2018) attributed the chloride sources of Melpitz during winter to the resuspension of road salt used for the de-icing of streets, mainly coming from the cities of Torgau and Leipzig. These sites are also located in the wind directions along with the coal and wood combustion emission region, which could explain the highest mass concentration of chloride during the winter. Furthermore, the existence of chloride might be due to low mass concentration marine influences consisting of sea-salt aerosol during all the seasons in the south-westerly direction (Fig. S2) which was previously studied by Stieger et al., (2018). However, it is known that the AMS-technology cannot properly detect sea salt (S. Huang et al., 2018; Ovadnevaite et al., 2014) because the majority of chloride is in the refractory part which cannot be flash vaporized at 600 ºC. Consequently, the chloride detected by the ACSM is mostly related to combustion processes (wood, coal combustion as well as trash burning; Li et al., 2012).

3.1.2 eBC and organics

The eBC showed its maximum mass concentration and mass fraction to PM mass during winter time at 1.38 µg/m^3 and 9 %, respectively (Fig. 2), and only 0.25 µg/m^3 and 4 %, respectively, during summer time (Fig. 2). This is consistent with the expected highest anthropogenic emissions from fossil fuel consumption (house heating and energy productions) in winter compared to summer (Spindler et al., 2010). Furthermore, considering measured eBC in regard to wind speed and wind direction (Fig. S2), the highest mass concentrations could be linked to north-easterly and south-westerly winds for fall, winter, and spring seasons, while in summer time it is mostly linked to the surrounding emissions (Fig. S2). Significant changes in the diurnal profiles of eBC for the different seasons can be found with the highest mass concentrations throughout the cold months compared to warm months owing to house heating (Fig. 3). It also showed morning and evening peaks during all seasons (Fig. 3). This is consistent with those observed for the nitrogen oxides (Fig. S3), which might be attributed to liquid fuel emissions and possibly the impact of the traffic rush hours on the main street, B 87, located approximately 1 or 1.5 km north of the station, (Yuan et al., 2021). In the following chapter, diurnal patterns showed lower mass concentrations at noon, and increased in the late afternoon to become nearly constant from 8 p.m. until midnight (Fig. 3). This ambient particulate pollution resulting from very surrounding sources in the village was reported by van Pinxteren et al., (2023). Diurnal increments of eBC were smaller in fall and spring compared to winter; the increment in summer is also correspondingly low due to the absence of house heating emissions, and the diurnal variation in the increment is determined by surrounding motor vehicle emissions in

https://doi.org/10.5194/acp-2022-842
Preprint. Discussion started: 11 January 2023


Atmospheric Chemistry and Physics Discussions

combination with the mixing layer height (van Pinxteren et al., 2023). Further discussions on the seasonal trend of the eBC can be found in Sect. 3.3.

Organic aerosol (OA) was the predominant species throughout the whole year, with a mean mass concentration of 4.84 µg/m^3 and a mass fraction of 46 % (Fig. 1c; Table. 1). The OA mass fraction decreased from the maximum value in summer and attained a minimum mass fraction in winter (58 %, 39 %, respectively; Fig. 2b). Similar to the comparison of previous inorganic AMS measurements performed at Melpitz (Poulain et al., 2011), AMS-OA contribution to total PM_1 showed maximum contribution during summer (59 %, Table. S1), and minimum contribution during winter (23 %) as well. However, the mass concentration of OA increased from its lowest value in summer and reached its highest value in winter time (3.67 µg/m^3, 6.21 µg/m^3 respectively; Fig. 2, Table. 1). Similar to eBC, OA measured in according to wind direction and wind speed showed highest average mass concentrations for north-easterly and south-westerly winds in winter (Fig. S2). In fall, polluted air masses came from the north-easterly direction, and in spring and summer OA, surrounding emissions closer to Melpitz were identified (Fig. S2). The diurnal cycle of the organic had an identical pattern across all seasons (Fig. 3), showing the highest mass concentration night time, a small peak in the early hours of the morning related to rush hours, and the lowest mass concentrations around the early afternoon. The peak observed around 12:00 UTC in summer time (Fig.3) can be due to the local photochemical production that leads to the formation of secondary organic aerosol mass during the day, similar to the diurnal behavior of sulphate (previously discussed in Sect. 3.1.1). However, the reduction in total OA mass concentration throughout the day (Fig. 3), which was mostly observed during the warm seasons (spring and summer), could be clearly related to the dilution effect of increasing mixed layer height.

Overall, eBC and OA can be composed of various sources with strong seasonal dependencies, as well as be influenced by different responses to atmospheric dynamics depending on meteorological parameters, geographical locations, and chemical processes. Therefore, a comprehensive analysis of the OA and eBC sources was performed using source apportionment techniques.

3.2 Source apportionment of OA

The chosen solution for the organic aerosol source apportionment contained five different factors based on their time series and mass spectra (Fig. 4). The source apportionment solution is based on a partly constrained rolling approach with three primary organic factors (POA), namely HOA (on average 0.30 µg/m^3 and 6 % of the total OA; Table.1 and Fig. 4), BBOA (on average 0.39 µg/m^3 and 7.9 % of the total OA) and CCOA (on average 0.77 µg/m^3 and 15.4 % of the total OA). In addition to these POA factors, two oxygenated organic aerosols (OOAs) were identified as LO-OOA (on average 1.62 µg/m^3 and 32.4 % of the total OA), and MO-OOA (on average 1.92 µg/m^3 and 38.4 % of the OA). The seasonal average mass concentrations and relative mass fractions of each OA factor to the total OA mass and their seasonal diurnal variation are presented in Figures 5 and 6; respectively. They will be discussed separately in the following sections.

https://doi.org/10.5194/acp-2022-842
Preprint. Discussion started: 11 January 2023


Atmospheric Chemistry and Physics Discussions

321 **3.2.1 POA factors**

322 The HOA mass spectrum (Fig. 4b) is recognized by mass fragments at unsaturated and saturated hydrocarbon chain pairs *m/z*
323 41 (C_3H_5), 43 (C_3H_7), *m/z* 55 (C_4H_7) and 57 (C_4H_9) (Zhang et al., 2005; Canagaratna et al., 2004), which are representative of
324 liquid fuel combustion emissions and are associated with either traffic emissions or domestic heating fuel (Wang et al., 2020).
325 This result designates HOA as a minimal source of OA at the monitoring site, which is consistent with previous studies in the
326 PM_1 range made in the same place: a) total average was 7 % of the organic mass concentration in a study by Crippa et al.,
327 (2014) total average was 3 % of PM size range between 0.05-1.2 µm mass concentration in a study by van Pinxteren et al.,
328 (2016) (Table. S2). However, in comparison with other ACSM/AMS stations in Europe (22 stations; Chen et al., 2022),
329 Kosetice with 9.7 % as a rural-background site, and Bucharest with 13.7 % as an urban-background site showed the minimum
330 annual HOA mean contribution of total OA, which is similar to the contribution at Melpitz.
331 Mass concentration of HOA followed a slightly increasing seasonal pattern towards the cold months, from 0.23 µg/m^3 in
332 summer to 0.36 µg/m^3 in the winter (Fig. 5a; Table. 1). HOA presented a low correlation with nitrogen oxides over the entire
333 period (R^2= 0.17, Table. 1), but it correlated well with eBC in winter (R^2= 0.52; Table. 1) and shows a weaker correlation in
334 summer (R^2= 0.28; Table. 1). Possibly HOA is also associated with household heating (35 % by oil and 11 % by liquid
335 petroleum gas, van Pinxteren et al., 2023) rather than traffic emissions, especially during the cold months. Analyzing the
336 pollution wind rose, the highest winter HOA mass concentrations are associated with the north-easterly wind direction
337 regardless of the wind speed suggesting the influence of long-range transported emissions (Fig. 7). During the warm months,
338 the emissions were more from the surrounding area, still associated with a north-easterly wind direction but only at low wind
339 speed (Fig. 7), which might be associated with either the surrounding traffic emissions, as well as the domestic emissions
340 associated not with house heating in summer but with hot water production (van Pinxteren et al., 2023).
341 The diurnal patterns of HOA reproduced two peaks in the morning and evening for all seasons (Fig. 6). The small time shift
342 for the start of the evening increase corresponds to the time shift of the sunrise between winter and summer. The diurnal cycles
343 reached a systematic minimum during the day time probably not only owing to emission decrease but also emphasizing the
344 effect of dynamic atmospheric processes (e.g. mixing layer height (MLH) and planetary boundary layer (PBL)) (Fig. 6, and
345 S4). Oppositely to what can be seen during the day time, night time mass concentrations appeared to be unaffected by the
346 seasons, showing similar mass concentrations all year round, i.e. their mass concentration rose continuously in the early
347 evening and remained at a very similar mass concentration over the night, which supports the hypothesis of yearlong
348 continuous rather surrounding emissions.
349
350 The mass spectra of BBOA are identified by ions at *m/z* 29, 43, 60, and 73 (Fig. 4b), known as fragments tracers of anhydro-
351 sugars like levoglucosan (Alfarra et al., 2007), which have been identified as indicators of wood combustion processes
352 (Simoneit et al., 1999; Simoneit and Elias, 2001). This is confirmed by the correlation between BBOA and levoglucosan over
353 the whole period (R^2= 0.65; Table. 1). On average, BBOA mass concentration and contribution were 0.39 µg/m^3 and 7.9 %,

https://doi.org/10.5194/acp-2022-842
Preprint. Discussion started: 11 January 2023


Atmospheric Chemistry and Physics Discussions

354 respectively (Table. 1 and Fig. 4a). However, its contribution is highest during winter time (10.6 %; Fig. 5), which is similar
355 to previous studies in different PM ranges for the Melpitz station during the cold months: a) in PM_1 range, 14 % of OA mass
356 concentration in fall (Crippa et al., 2014); b) in 0.05-1.2 µm range, highest contribution with 10 % of PM mass concentration
357 in winter (van Pinxteren et al., 2016); and c) in PM_{10} range, highest contribution with 16 % of PM mass concentration in winter
358 (van Pinxteren et al., 2023).
359 The high value of BBOA is mainly attributed to residential heating, and indicates the effect of transported biomass burning
360 emissions to the sampling site in cold months (Fig. 7), while in summer time, it is still observable as surrounding emissions
361 during periods of low wind speed (Fig. 7 and Fig. S4) with a mass concentration of 0.21 µg/m^3 and a contribution of 6.1 % to
362 total OA (Fig. 5). The presence of BBOA in the summer can be linked to water heating systems using wood briquettes and
363 logs (estimated at 32 % of total central heating in this area, van Pinxteren et al., 2023). Moreover, it can also be related to
364 recreational open fires and/or barbecue activities (van Pinxteren et al., 2023). This result is similar to other ACSM/AMS rural-
365 background stations in Europe (22 stations; Chen et al., 2022); both Magadino and Kosetice showed the highest contribution
366 of BBOA during winter time (27.4 % and 15.5 % respectively).
367 The diurnal cycles, peaking from early evening to early morning in winter (Fig. 6), match the expectations for a factor related
368 to domestic heating activities, along with a better eBC correlation during winter than during summer time (R^2= 0.81, and R^2=
369 0.42, respectively; Table. 1). Finally, in opposition to HOA, the night time BBOA mass concentration showed a strong seasonal
370 variation having its highest mass concentration during winter nights and lowest during summer time, the influence of the
371 impact of house heating emissions on the BBOA emissions. However, the day time behavior reflects the influence of enhanced
372 vertical mixing during day time (higher temperature, Fig. S3) combined with high wind speeds (Fig. 11) can readily cause
373 dilution and thus low pollutant concentrations near the ground (Chen et al., 2021; Via et al., 2020; Paglione et al., 2020).
374
375 The mass spectrum of CCOA is characterized by fragments at *m/z* 77, 91, and 115 (Fig. 4b) as previously reported by Dall'Osto
376 et al., (2013); Xu et al., (2020); Tobler et al., (2021) and Chen et al., (2022). These specific fragments can be associated with
377 unsaturated hydrocarbons, particularly ion peaks related to polycyclic aromatic hydrocarbon (PAH). The CCOA time series
378 showed the strongest correlation with eBC (R^2= 0.9; Table. 1). In addition, several studies reported that coal combustion
379 emissions are often accompanied by high chloride mass concentration (e.g; Iapalucci et al., 1969; Yudovich and Ketris, 2006
380 and Tobler et al., 2021). Here, the correlation between CCOA and chloride was higher during winter than during summer time
381 (R^2= 0.41, 0.15 respectively; Table. 1), as the gas-particle phase equilibrium dramatically changes with rising temperatures
382 (Tobler et al., 2021). Although chloride is almost observable in the particle phase as ammonium chloride (NH_4Cl) at lower
383 temperatures, chloride is typically observable in the gas phase as hydrogen chloride (HCl) at higher temperatures (Tobler et
384 al., 2021).
385 CCOA represented on average 15.4 % of the total OA (0.77 µg m^{-3}), (Table. 1; Fig. 4a) and is the most important POA over
386 the entire period. No CCOA factor was identified in the previous AMS measurements made at Melpitz (Crippa et al., 2014).
387 Most likely this factor was not properly resolved and/or it was not possible to properly separate it from the other factors since

https://doi.org/10.5194/acp-2022-842
Preprint. Discussion started: 11 January 2023


Atmospheric Chemistry and Physics Discussions

no reference mass spectra for CCOA was reported in the literature at that time. CCOA showed the highest mass concentration and mass fraction during the winter (1.58 µg/m^3, 23 %, respectively; Fig. 5a; Table. 1), which is related to the surrounding emissions and long-range transported air masses coming from two different directions, north-easterly and south-westerly (Fig. 7). Not surprisingly, the lowest mass concentration and contribution were observed during the summer time (0.30 µg/m^3, 8.7 %, respectively; Fig. 5a; Table. 1,) which most probably correspond to only long-range transport as later discussed in Sect. 3.4 (Fig. 9). Moreover, this result is consistent with previous measurements made in the same place. For the size range 0.05-1.2 µm van Pinxteren et al., (2016) reported a contribution of 29 % and 21 % of the PM in winter and summer respectively, and a contribution of 7 % and 0 % for winter and summer respectively for the PM_{10} range was found (van Pinxteren et al., 2023). From all ASCM/AMS stations (22 stations; Chen et al., 2022) only Melpitz as a rural-background site and Krakow as an urban-background site showed the coal combustion emissions with the maximum contribution during winter for both sites (Krakow: 18.2 % and Melpitz: 23 %) compared to summer (Krakow: 4.5 % and Melpitz: 8.7%). The drastic seasonal changes in Krakow are attributed to the common use of coal burning for residential heating reasons during the winter time (Casotto et al., 2022; Tobler et al., 2021), while in Melpitz, as discussed above, coal combustion is affected by both surrounding and transported emissions from other sites.

Mass concentrations of CCOA during night time were much higher than during day time throughout all seasons (Fig. 6), further verifying the increased coal combustion emissions from coal heat generation at winter time night and the potential decrease in emissions during the day due to a strong influence of atmospheric dynamics.

3.2.2 OOA factors

The two OOAs (Fig. 4) referred to as LO-OOA and MO-OOA are known to be characterized by the different ratios of their *m/z* 43 and *m/z* 44 fragments (Fig. 4b), that represent the oxidation level (Canagaratna et al., 2015). While *m/z* 43 could be derived from $C_2H_3O^+$ (a signature of the semi-volatile) and/or C_3H7^+ (a signature of the primary emissions of the hydrocarbon-like), *m/z* 44 is mainly derived from the fragment of CO_2^+ (a signature of oxygenated, particularly acids) (Canonaco et al., 2015; Ng et al., 2010). As presented in Fig. 4b, MO-OOA mass spectra showed a notable peak at *m/z* 44. This spectrum has been extensively recognized as low volatility OOA (LV-OOA) and described to be made up of aged secondary OA (SOA) and highly oxidized OA (Lanz et al., 2007; Ulbrich et al., 2009; Q. Zhang et al., 2011; Ng et al., 2011b); while the mass spectra of LO-OOA in this study presented a higher *m/z* 43 (Figs. 4b) compared to MO-OOA, which is similar to the mass spectral pattern of the previously reported freshly formed semi volatile OOA (SV-OOA) (Jimenez et al., 2009; Ng et al., 2010). To differentiate the variations of OOAs factor, the *f*44 vs *f*43 space was used which is a typical diagnostic tool based on atmospheric aging (Ng et al., 2010).

The seasonal *f*44/ *f*43 for OOAs measured points and the *f*44/ *f*43 for modelled factor profiles (LO-OOA and MO-OOA) are presented in Fig. S4. The data points in Fig. S4 are distributed differently according to the season (Chen et al., 2021; Canonaco et al., 2015; Crippa et al., 2014; Chazeau et al., 2022). Furthermore, the modelled factor profile points represent a high variability in space, especially for LO-OOA. This assumes how an annual or seasonal PMF solution, unless a larger number

https://doi.org/10.5194/acp-2022-842
Preprint. Discussion started: 11 January 2023


Atmospheric Chemistry and Physics Discussions

of factors are used, would perform poorly in capturing all of the variations of SOA. In order to capture time-dependent changes, in particular for LO-OOA, it is, therefore, advantageous to perform rolling PMF analysis. The triangle plot defined by Ng et al. (2010) is also shown in Fig. S4. As assumed the LO-OOA points were concentrated in the lower part of the space, whereas more aged MO-OOA points relocated to the upper part of the space during the aging process. The fall, spring, and summer data points were all located on the right side of the triangle (Fig. S4), however the winter data points were located near the top and inside the triangle. The data points on the right side of the triangle correspond to the time exposed to higher temperatures more than those that are within the triangle. This could be attributed to an increase in biogenic SOA emissions if the temperature increased, as biogenic OOA appears to be dispersed all along right the side of the triangle. Further, as the temperature is reduced, the increased biomass emissions cause the OOA points to lie vertically inside the triangle, as seen in the winter data.

The two OOAs were the two most significant contributors to the total OA fraction (Fig. 4) over the entire period. The seasonal mean mass concentrations of MO-OOA varied from higher mass concentrations during winter (2.25 μg/m^3) and lower during summer time (1.44 μg/m^3, Table. 1). However, the highest MO-OOA mass concentrations found during the cold periods are similar to the seasonal patterns in POA. Furthermore, high mass concentrations of MO-OOA are generally found at high relative humidity (RH > 80 %) and low temperature (< 0 ˚C), i.e., conditions during winter time (Fig. S5). This low air temperature condition can be linked to a possible scenario for an increase in the MO-OOA precursor emissions from biomass burning and coal combustion as a result of residential heating activities during winter time. Therefore, significant enhancement appears to be an effect of RH during winter, proposing that the aqueous-phase heterogeneous mechanisms could also play a crucial way in the regional MO-OOA formation through winter as suggested by Gilardoni et al., (2016). In contrast, no RH-temperature-dependent trends for the MO-OOA were found in the other seasons (Fig. S5), indicating more complex formation processes during other seasons. Meanwhile, MO-OOA diurnal cycles presented a seasonal variation as well, with a remarkable enhancement in the evening and night time during winter (Fig. 6), indicating a potential regional formation mechanism containing night time chemistry (Tiitta et al., 2016). While in fall, spring and summer, MO-OOA displayed a considerable increase during the day (Fig. 6), indicating that higher temperatures result in considerable regional photochemical production of SOA particles (Fig. S3) and enhanced solar radiation (Petit et al., 2015). Furthermore, regarding the correlation of mass concentration of MO-OOA with sulphate, the latter is regarded as a local secondary production indicator (Petit et al., 2015, and Table. 1). Consequently, alongside almost stable mass spectra throughout the year, MO-OOA seems to be derived from a variety of seasonal-dependent formation mechanisms and sources (such as aged background, biomass burning, coal combustion, and biogenic sources).

The seasonal mean mass concentrations of LO-OOA varied from higher mass concentrations during fall (2.13 μg/m^3) and lower mass concentrations during spring time (1.24 μg/m^3, Table. 1). Temperature had a significant effect on LO-OOA, and showed a distinguishable seasonal variation pattern. The temperature-RH dependence of the LO-OOA was not quite similar depending on the season (Fig. S5). The highest winter time LO-OOA mass concentrations were found mostly at low

https://doi.org/10.5194/acp-2022-842
Preprint. Discussion started: 11 January 2023


Atmospheric Chemistry and Physics Discussions

455 temperatures and high RH environments, indicating that gas-particle partitioning might have a key role in LO-OOA formation
456 throughout this season. The freshly formed SOA deriving from primary biomass burning and coal combustion emissions, as
457 found in previous studies (Crippa et al., 2013; Zhang et al., 2015; Y. Sun et al., 2018; Stavroulas et al., 2019) can also affect
458 the LO-OOA during the cold months. Furthermore, during winter time the correlations between LO-OOA and nitrate (R^2=
459 0.59) were found. Different LO-OOA daily cycles were also found in different seasons (Fig. 6). The daily changes in LO-
460 OOA displayed higher mass concentrations in night time compared to day time in fall, spring, and summer (Fig. 6), highlighting
461 the significant roles of night time chemistry and/or gas-particle partitioning in the LO-OOA formation, while the decrease
462 during the day is partly linked to the atmospheric dilution effect (Fig. S3), evaporation and photochemical aging into MO-
463 OOA (Fig. 6). For winter night increments, lower temperature in favor of condensation; and more abundant precursors present
464 considering increased BBOA emission, therefore enhanced night chemistry activities, leads to higher LO-OOA; moreover,
465 shallow boundary layer in winter and night time inversion caused pollutants to accumulate.

466 **3.3 eBC source apportionment**

467 The eBC correlated with each of the three identified primary organic factors (HOA, BBOA, and CCOA) during the source
468 apportionment analysis (Table. 1). The total amount of these primary factors (known as POA) was highly correlated with eBC
469 (R^2= 0.87; Fig. 8a). As a result, the different sources of eBC were evaluated for each factor utilizing a multilinear regression
470 model, as suggested by Laborde et al., (2013); Zhu et al., (2018) and Poulain et al., (2021), for instance. The following assumes
471 that the eBC mass is associated with the separate contribution from each OA factor (i.e., eBC_{HOA}, eBC_{BBOA}, and eBC_{CCOA}) at
472 any time:
473
474 $$eBC(t) = eBC_{HOA}(t) + eBC_{BBOA}(t) + eBC_{CCOA}(t) \quad (3)$$
475
476 The eBC emission from each source is expected to be proportionate to the separate source mass concentration generated in
477 each season (m_{HOA}, m_{BBOA}, and m_{CCOA}, respectively). As a result, the multilinear regression model can be described as follows:
478
479 $$eBC(t) = am_{HOA} + bm_{BBOA} + cm_{CCOA} \quad (4)$$
480
481 where a, b, and c are the linear regression coefficients for m_{HOA}, m_{BBOA}, and m_{CCOA}, respectively, that will be applied to evaluate
482 the contribution of eBC per each POA factor for each season (Table. S3).
483 CCOA appeared to have the largest source of eBC, contributing half of it (eBC-CCOA 55 %, Table. 1), followed by eBC
484 associated with BBOA 37 % (eBC-BBOA), while the lowest contribution was found for eBC-HOA (8 %). However, the
485 contribution of sources to the total eBC strongly depends on the season. Looking at each individual source, the hydrocarbon-
486 like emissions contributed most to the eBC fraction in the fall (eBC-HOA with 22 %, Table. 1; Fig. 8b), while biomass burning
487 emissions dominated the eBC in summer and coal combustion emission dominated in winter (eBC-BBOA and eBC-CCOA

https://doi.org/10.5194/acp-2022-842
Preprint. Discussion started: 11 January 2023


Atmospheric Chemistry and Physics Discussions

with 69 % and 56 %, Table. 1). In the diurnal cycle, contribution to the total eBC of eBC-HOA showed two peaks in the morning and evening for fall, spring and summer (Fig. S6), reflecting the impact of the traffic rush hours as mentioned in Sect. 3.2.1, and the minimum contributions during the day time due to the effect of lowest emissions and PBL effect (Fig. S3). However, winter time did not show a strong variation in the diurnal cycle (Fig. S6). This indicates the potential influence of continuous emissions at the measurement site. Biomass burning combustion with its maximum contribution during the day in summer (Fig. S6) can be related to a variety of different eBC-POA mass concentrations (Fig. S6b), while the BBOA mass concentration was almost constant, the other POA mass concentration decreased during the day. Coal combustion showed an increasing contribution during night time in all the seasons (Fig. S6), especially during the winter time, which further confirms the enhanced coal combustion emission in winter nights (Fig. S6b).

3.4 Impact of air mass origin and trajectory analysis

As mentioned before, the geographical origin of the PM_1 chemical species and also PMF components are not only emitted from the surrounding area but transported. Therefore, to better identify the origin of their sources, trajectory analysis, and their clustering analysis were applied using the self-developed back-trajectory cluster method (BCLM) (Sun et al., 2020; Ma et al., 2014; Hussein et al., 2006). A total of fifteen clusters were identified, corresponding to different meteorological conditions over the course of the year at Melpitz (Fig. 9a). The different clusters can be divided according to the different seasons (CS: cold season; TS: transition season; and WS: warm season), and meteorological synoptic patterns (ST: stagnant; A1: anticyclonic with air mass coming from Eastern Europe; A2: anticyclonic with air mass coming from the west; C1: cyclonic with air mass coming from relatively south; C2: cyclonic with air mass coming from the west and south west). However, the clustering approach did not consider spring and fall separately, and therefore the transition clusters correspond to both spring and fall. Regarding this cluster approach, six air masses were identified for the winter season, four air masses for the transition seasons, and five air masses for the summer season. The number of clusters with their corresponding mean mass concentration of PM_1 chemical species and PMF factors of organics are summarized in Table. 2 and with more details in Tables S3 and S4.

3.4.1 Winter

Fig. 9b and 9c illustrate the mass concentration and contribution of PM_1 chemical species and PMF factors of organic for each air mass type at Melpitz based on the type of air masses. For the winter season, the cluster CS-ST corresponds to more surrounding emission origin with a PM mean value of 21.95 $\mu g/m^3$, which occurred during 14 % of the total measurement period. This cluster with the highest mass concentration of LO-OOA to the PM mass (2.73 $\mu g/m^3$) could confirm the role of freshly formed SOA originating around the station from primary biomass burning and coal combustion emissions (mass concentration of 0.97 $\mu g/m^3$ and 1.89 $\mu g/m^3$, respectively). Furthermore, nitrate showed a high mass concentration and contribution in this air mass (5.38 $\mu g/m^3$ and 25 %, respectively) due to e.g., meteorological conditions and abundant precursors.

https://doi.org/10.5194/acp-2022-842
Preprint. Discussion started: 11 January 2023


Atmospheric Chemistry and Physics Discussions

The cluster CS-A1 with the highest mass concentration of PM (29.14 µg/m^3) represented Eastern European continental air masses (passing Poland and the Czech Republic) during anticyclonic flow which occurred during 18 % of the total measurement period, meaning that Melpitz was under their influence during winter. This air mass, with the highest POA mass concentration (5.56 µg/m^3), especially coal combustion emissions (CCOA and eBC-CCOA with an average mass concentration of 4.01 µg/m^3 and 1.93 µg/m^3, respectively), highlight the importance of long-range transported emissions. This cluster also contained the highest mass concentration of sulphate (5.39 µg/m^3) and can support the importance of coal combustion on sulphate formation, which is known to be strongly emitted by coal power plants (Wierońska-Wiśniewska et al., 2022).

The air mass CS-A2 identified as marine-influenced air with a mean value of 13.39 µg/m^3 of PM came from the United Kingdom with the anticyclonic flow, which occurred during 8 % of the total measurement period. This cluster presented a low mass concentration of POA and for two OOAs almost the same mass concentration and contribution (Table. S3 and Table. S4). Since Melpitz is placed away from the coast, therefore the sampling location is affected by aged maritime air masses (Poulain et al., 2011). Inorganics are dominated by nitrate in this cluster with the high mass concentration (3. 86 µg/m^3) and represent the highest mass fraction (50 % of the total inorganic species).

The CS-C1 air mass with a mean value of 15.99 µg/m^3 characteristic of Southern European air mass, came from an industrial and polluted area starting from Spain and partly crossing Italy with the cyclonic flow, which occurred during 10 % of the total measurement period. POA mass concentration and contribution were low in this cluster, while SOA, especially MO-OOA, showed the highest mass concentration of PM over the entire period (3.77 µg/m^3) and the highest contribution during the winter season (24 %). This can be linked to the high sulphate in this air mass (2.99 µg/m^3), which showed that the regional influence by contribution from aged BBOA and CCOA might manifest in MO-OOA (as discussed in Sect. 3.2.2).

Finally, CS-C2a and CS-C2b were both associated with cyclonic and marine influence conditions which only occurred for a short time (3 % and 2 % of the total measurements, respectively), showing the lowest PM mean value (4.09 µg/m^3 and 2.60 µg/m^3, respectively). Both of them showed almost the same mass concentration and contribution of POA (Fig. 8a and b; and Table. S3 and S4). However, similarly to CS-A2, cluster CS-C2a contained a marine component at the beginning point of the air masses, and in the following time it was dominated by continental areas (France and southern Germany), where due to the longer time transferring over continent and aging process, it showed more nitrate mass concentration and contribution than CS-C2b (1.35 µg/m^3, 16 µg/m^3; and 28 % 14 %, respectively). Whereas CS-C2b started near Iceland with same history of the air mass over the continent, and in comparison, with CS-C2a, it presented a higher contribution of sulphate (29 % and 19 %, respectively), which could be associated with aged marine air mass due to the higher contribution of MO-OOA (21 % and 18 %, respectively).

3.4.2 Transition seasons

For transition seasons (fall and spring), whereas the four clusters showed a quite similar PM mass concentrations (Fig. 9) which might be linked to the overall weather situation during these two times of the year, their chemical composition strongly

https://doi.org/10.5194/acp-2022-842
Preprint. Discussion started: 11 January 2023


Atmospheric Chemistry and Physics Discussions

depended on their origins. TS-A1 and TS-A2 corresponded to two different types of anticyclonic air masses with respective mean PM mass concentrations of 6.06 µg/m^3 and 5.86 µg/m^3. Cluster TS-A1 which occurred during 4 % of the total measurements period, started from Finland, crossing the Estonian, Latvian, Lithuanian and Polish coasts before arriving at Melpitz. Although it might contain a certain marine component, this cluster mostly followed coastal areas, which means that in this cluster OA mass concentration dominated PM (2.95 µg/m^3). Furthermore, this cluster showed continental and polluted aspects with the highest LO-OOA mass concentration and contribution during transition seasons (1.03 µg/m^3 and 17 % respectively), which is linked to originating from freshly formed SOA from primary biomass burning and coal combustion emissions around coastal areas. On the other hand, cluster TS-A2 (4 % of the measurements period) is characterized as a marine cluster and started from the south of Iceland/Greenland. This cluster showed inorganic as the dominant PM with a high mass concentration and a mass fraction (3.35 µg/m^3 and 58 % respectively). Since Melpitz is influenced by aged marine air masses, this cluster showed a maximum nitrate mass concentration during the transition seasons (1.54 µg/m^3 and a contribution of 26 %, respectively).

Finally, two other clusters TS-C1 and TS-C2 were two different types of cyclonic air masses in fall and spring time, with mean PM mass concentrations of 4.69 µg/m^3 and 4.94 µg/m^3 respectively. These trajectories with different types of marine influenced air masses occurred for a very short period of time (3 % and 4 % of the total measurements period, respectively). The first one, TS-C1, started from the Atlantic Ocean near Spain and is associated with a more continental influence, which is why organic mass concentration and contribution were higher than inorganic. However, The LO-OOA contribution of this cluster was the highest during this time period (26 %) due to the aging processes of primary organic aerosols especially CCOA, which had a maximum mass concentration (0.31 µg/m^3 and mass fraction of 7 %, respectively). While the second one, TS-C2, was almost a pure marine cluster, coming from the Norwegian Sea. In opposition to TS-C1, PM was dominated by inorganics in TS-C2, with a high mass concentration of nitrate (1.35 µg/m^3) representing the aging effect due to the long-time transfer over the continents.

3.4.3 Summer

During the summer season, the different clusters showed strong changes in both chemical composition and total mass concentration. Cluster WS-ST was identified as the local air mass with a mean value of 8.97 µg/m^3, which occurred for a short period, 6 % of the measurement. However, this cluster contained a low POA mass concentration but a maximum contribution of MO-OOA (32 %), assuming important regional photochemical roles of SOA particles with higher temperatures (Fig. 11) and enhanced solar radiation (Petit et al., 2015).

Air masses WS-A1 and WS-A2 were two different types of anticyclonic air masses with different directions and different mean PM mass concentrations. Cluster WS-A1, known as the highest mass concentration during summer time, (16.95 µg/m^3 and contribution of 11 % of the measurement period) was the continental air mass which was coming from Eastern Europe during the anticyclonic flow (starting from Belarus, crossing Poland and the Czech Republic). This air mass included maximum inorganic and organic especially CCOA mass concentration (1.28 µg/m^3) during summer time, which can explain the existing

https://doi.org/10.5194/acp-2022-842
Preprint. Discussion started: 11 January 2023


Atmospheric Chemistry and Physics Discussions

higher CCOA during summer, and showed the role of long-range transported emissions in the summer season. However, WS-A2 air mass, with a mean value of 9.48 µg/m^3 was a marine-influenced air masse and was coming from the North Sea, which only occurred for a short period (6 % of the total measurement period).

Moreover, two cyclonic air masses, WS-C1 and WS-C2, were also identified as two different marine clusters. These trajectories did not occur very often, only 5 % and 3 % of the total measurement period, respectively. The starting point of WS-C1 with a mean value of 8.41 µg/m^3 was the Celtic Sea, but in the following time, it predominantly passed over continental areas (France and southern Germany), which means it could be aged and the result can be shown in the high mass concentration of nitrate and sulphate in this cluster (1.63 µg/m^3 and 1.86 µg/m^3, respectively). Finally, the starting point of WS-C2 with a mean value of 4.46 µg/m3, was near Iceland, with the lowest PM mass concentration during summer. However, it showed the highest sulphate contribution (27 %) at this time which could be associated with aged marine air mass like other marine air masses.

3.4.4 Cluster seasonality

A parallel comparison can be made between the winter and summer clusters. Clusters CS-A1 and WS-A1 both show the highest POA contribution dominated by coal combustion, which emphasizes that the origin of this source could be associated with the transport of the coal power plants emissions from Eastern Europe (e.g. Eastern part of Germany, Poland, Czech Republic and further countries located in the East). They were not only affected by the winter air quality but also the summer air quality.

Clusters CS-ST and WS-ST, which were known as local air masses, showed the seasonal effect on the chemical component. First, the volatility of ammonium nitrate at higher summer temperatures could explain their lower value in summer. Then, atmospheric photochemical oxidation processes affected the sulphate locally formed emission in summer, which its highest value over inorganic components during summer can confirm. Not surprisingly, due to the residential heating effect, POA mass concentration was very high during winter; however, freshly formed SOA originating from biomass and coal emissions can explain the higher LO-OOA mass concentration in winter.

During the whole period, some marine air masses with cyclonic and anticyclonic flow showed the important roles of aged marine air masses over the measurement site: a) clusters CS-A2 and WS-A2 with anticyclonic pattern starting from the North and/or Norwegian Sea, and b) CS-C2a, WS-C1, and TS-C1 starting from the Celtic Sea near Spain, and also CS-C2b and WS-C2 starting from Iceland, all with cyclonic pattern contain nitrate and sulphate during the transferring over the continental areas in different seasons.

4 Conclusion

Within this study, the change in chemical compositions of non-refractory fine aerosol (NR-PM$_1$) at the German rural-background observatory Melpitz was investigated during a one-year period between September 2016 and August 2017, by applying PMF in a rolling fashion with 14 days window length and a 1-day shift using the SoFi Pro. This method provided the

https://doi.org/10.5194/acp-2022-842
Preprint. Discussion started: 11 January 2023


Atmospheric Chemistry and Physics Discussions

617 decomposition of time-dependent factor profiles that were able to better capture the variability of OA sources across seasons,
618 in particular for LO-OOA. Overall, the averaged total PM_1 mass concentration is 10.47 μg/m^3 and follows a clear seasonal
619 pattern, with the highest mass concentration during winter (15.95 μg/m^3) and lowest mass concentration during summer time
620 (6.24 μg/m^3). The organic aerosol was the major component accounting for 46 % of total PM_1 and showing a strong seasonal
621 variability ranging from 39 % (in winter) to 58 % (in summer). It was followed by sulphate (15 % and 20 %) and nitrate (24
622 % and 11 %). The final solution of the PMF rolling approach for OA source apportionment enabled the identification of five
623 factors throughout the one-year measurements of OA; HOA, BBOA, CCOA, LO-OOA, and MO-OOA.
624
625 Generally, in Melpitz, HOA as a minor source of OA (6 % of the contribution of total organic mass) was associated with: a)
626 low traffic emissions, b) household heating in winter, and c) the central heating for hot water production for all the seasons
627 which showed a small increasing mass concentration pattern toward cold months (winter and summer: 0.36-0.23 μg/m^3). The
628 HOA night time mass concentration was not affected by the seasons, which indicates the presence of a continuous emission
629 source. Biomass burning emissions (BBOA) representing 7.9 % of the contribution of total organic mass showed a seasonal
630 effect, emphasizing the impact of house heating during winter (winter and summer: 23 % and 8.7 %). This highest mass
631 concentration during the winter time showed the descending pattern from night time to day time due to domestic heating
632 activities and the planetary boundary layer effect; however similar to HOA, the presence of BBOA during summer was due to
633 central heating which uses multiple fuel types in the Melpitz area. The most dominant anthropogenic source was associated
634 with coal combustion (CCOA) with a 15.4 % contribution of total organic mass and 55 % of eBC with the highest mass
635 concentration and contribution of PM during winter rather than summer (1.58-0.30 μg/m^3). Although a certain fraction of
636 CCOA could be linked to surrounding domestic heating (van Pinxteren et al., 2023), it is rather associated with power plant
637 emissions and long-range transport all year round. Using the correlation between HOA, BBOA, and CCOA with eBC, a
638 multilinear regression approach was applied to perform the source apportionment of eBC. This analysis highlighted eBC
639 contribution related to the source of HOA (8 % of the total eBC), BBOA (37 % of the total eBC), and CCOA (55 % of the
640 total eBC), which showed the CCOA as the largest source of eBC during the measurement period. Moreover, from the seasonal
641 source apportionment, CCOA presented the largest fraction (56 % of the total eBC) during winter, while the highest fraction
642 is attributed to BBOA for summer time (69% of the total eBC). LO-OOA and MO-OOA referred to oxidized oxygenated
643 organic aerosol (32.4 % and 38.4 % of the contribution of total organic mass, respectively), were identified as a secondary
644 organic aerosol with the highest mass concentration during the cold months (fall: 2.13 μg/m^3 and winter: 2.25 μg/m^3,
645 respectively) and the lowest mass concentration during the warm months (spring: 1.24 μg/m^3 and summer: 1.44 μg/m^3,
646 respectively). LO-OOA mass concentration decreased during the day due to dilution, and the evaporation process resulted in
647 aging into MO-OOA.
648
649 A combination of pollution wind rose and cluster analysis was used to better understand the origin of the aerosol reaching the
650 station. Overall, Melpitz is influenced by fifteen types of air masses, such as long-range continental, marine, and surrounding

651 emissions. During winter and summer time, easterly continental air masses, CS-A1 and WS-A1 with an anticyclonic pattern
652 come from Eastern Europe and showed a significant particle mass concentration, especially high POA (and CCOA) mass
653 concentration at the measurement site. Marine clusters, mostly coming from the south/west/north side with aged marine air
654 masses including nitrate and sulphate, also have important roles in the PM mass concentration at the Melpitz site over the
655 entire period (winter: CS-A2, CS-C2b, and CS-C2a, transition: TS-C, TS-A2 and TS-C2, and summer: WS-Ca, WS-C2, and
656 WS-A2). However, the surrounding emissions are recognized as another important source of emissions which include high
657 organic and inorganic components during winter and summer (CS-ST and WS-ST, respectively).
658
659 Our results emphasize the importance of the long-range transported emissions of coal combustion related aerosol particles
660 regardless of the season, which supports that the main CCOA source is related to coal power plants emissions. However, coal
661 power plants emissions not only affect the surrounding air quality but can also be transported over long distances. It is important
662 to note that the overall coal combustion mass concentration presented here can certainly be underestimated since the identified
663 CCOA factor is associated with freshly emitted organic aerosol and no factor associated with potential aged coal combustion
664 was identified. Because coal still is an important energy source in the European energy mix (68.4 % of all energy in the EU
665 was produced from coal, crude oil, and natural gas, Energy Statistics - an Overview - Statistics Explained, 2022) as well as on
666 a global scale and also that it still will be in used for the coming decades (until 2040, Europe's Coal Exit - Europe Beyond
667 Coal : Europe Beyond Coal, 2022), further research should be done on the identification of coal emissions across Europe in
668 order to better understand its atmospheric aging processes.
669

670 **Acknowledgements**

671 This work is supported by the COST action CA16109 Chemical On-Line cOmpoSition and Source Apportionment of fine
672 aerosoLs (COLOSSAL), the SNF COST project SAMSAM IZCOZO_177063., by the infrastructure projects ACTRIS (EU
673 FP7, grant 262254), the RI-URBANS project under grant NO. 101036245, the ERA-PLANET, and transnational projects
674 SMURBS and iCUPE (grant agreement NO. 689443), and ACTRIS-2 (Grant 654109).
675

676 **References**

677 Aas, W., Tsyro, S., Bieber, E., Bergström, R., Ceburnis, D., Ellermann, T., Fagerli, H., Frölich, M., Gehrig, R.,
678 Makkonen, U., Nemitz, E., Otjes, R., Perez, N., Perrino, C., Prévôt, A. S. H., Putaud, J. P., Simpson, D., Spindler,
679 G., Vana, M., and Yttri, K. E.: Lessons learnt from the first EMEP intensive measurement periods, Atmos. Chem.
680 Phys., 12(17), 8073–8094, https://doi.org/10.5194/acp-12-8073-2012, 2012.
681 Alfarra, M. R., Prevot, A. S. H., Szidat, S., Sandradewi, J., Weimer, S., Lanz, V. A., Schreiber, D., Mohr, M., and
682 Baltensperger, U.: Identification of the mass spectral signature of organic aerosols from wood burning emissions,
683 Environ. Sci. Technol., 41(16), 5770–5777, https://doi.org/10.1021/es062289b, 2007.

https://doi.org/10.5194/acp-2022-842
Preprint. Discussion started: 11 January 2023

Allan, J. D., Delia, A. E., Coe, H., Bower, K. N., Alfarra, M. R., Jimenez, J. L., Middlebrook, A. M., Drewnick, F., Onasch, T. B., Canagaratna, M. R., Jayne, J. T., and Worsnop, D. R.: A generalised method for the extraction of chemically resolved mass spectra from Aerodyne aerosol mass spectrometer data, J. Aerosol Sci., 35(7), 909–922, https://doi.org/10.1016/j.jaerosci.2004.02.007, 2004.

Birmili, W., Heinke, K., Pitz, M., Matschullat, J., Wiedensohler, A., Cyrys, J., Wichmann, H. E., and Peters, A.: Particle number size distributions in urban air before and after volatilisation, Atmos. Chem. Phys., 10(10), 4643–4660, https://doi.org/10.5194/acp-10-4643-2010, 2010.

Birmili, W., Schepanski, K., Ansmann, A., Spindler, G., Tegen, I., Wehner, B., Nowak, A., Reimer, E., Mattis, I., M ¨ Uller, K., Brüggemann, E., Brüggemann, B., Gnauk, T., Herrmann, H., Wiedensohler, A., Althausen, D., Schladitz, A., Tuch, T., and Löschau, G.: A case of extreme particulate matter concentrations over Central Europe caused by dust emitted over the southern Ukraine, Atmos. Chem. Phys., 8, www.atmos-chem-phys.net/8/997/2008/, 2008.

Birmili, W., Stratmann, F., and Wiedensohler, A.: Technical note design of a DMA-based size spectrometer for a large particle size range and stable operation, J. Aerosol Sci., 30, Issue 4, 1999.

Birmili, W., Sun, J., Wiedensohler, A., Birmili, W., Sun, J., Weinhold, K., Merkel, M., Rasch, F., Spindler, G., Wiedensohler, A., Bastian, S., Löschau, G., Schladitz, A., Quass, U., Kuhlbusch, T. A. J., Kaminski, H., Cyrys, J., Pitz, M., Gu, J., Peters, A., Flentje, H., Meinhardt, F., Schwerin, A., Bath, O., Ries, L., Gerwig, H., Wirtz, K., and Weber, S.: Enhanced Land Use Regression models for urban fine dust and ultrafine particle concentrations View project Radon parallel measurements, View project Atmospheric aerosol measurements in the German Ultrafine Aerosol Network (GUAN), https://www.researchgate.net/publication/330910927, 2015.

Birmili, W., Weinhold, K., Rasch, F., Sonntag, A., Sun, J., Merkel, M., Wiedensohler, A., Bastian, S., Schladitz, A., Löschau, G., Cyrys, J., Pitz, M., Gu, J., Kusch, T., Flentje, H., Quass, U., Kaminski, H., Kuhlbusch, T. A. J., Meinhardt, F., Schwerin, A., Bath, O., Ries, L., Gerwig, H., Wirtz, K., and Fiebig, M.: Long-term observations of tropospheric particle number size distributions and equivalent black carbon mass concentrations in the German Ultrafine Aerosol Network (GUAN), Earth System Science Data, 8(2), 355–382, https://doi.org/10.5194/essd-8-355-2016, 2016.

Birmili, W., Wiedensohler, A., Mueller, K., Birmili, W., Weinhold, K., Nordmann, S., Wiedensohler, A., Spindler, G., Müller, K., Herrmann, H., Gnauk, T., Pitz, M., Cyrys, J., Flentje, H., Nickel, C., J Kuhlbusch, T. A., Löschau, G., Haase, D., Meinhardt, F., F., Schwerin, A., Ries, L., and Wirtz, K.: Atmospheric aerosol measurements in the German Ultrafine Aerosol Network (GUAN) Korngrößendifferenzierte Feinstaubbelastung in Straßennähe in Ballungsgebieten Sachsens (2003-2005) View project Chemistry, Air Quality and Climate View project Atmospheric aerosol measurements in the German Ultrafine Aerosol Network (GUAN) Part 1: Soot and particle number size distributions, https://www.researchgate.net/publication/232089057, 2009.

717 Bootstrap Methods: Another Look at the Jackknife on JSTOR, https://www.jstor.org/stable/2958830?origin=JSTOR-pdf, 1979.

719 Bressi, M., Cavalli, F., Putaud, J. P., Fröhlich, R., Petit, J. E., Aas, W., Äijälä, M., Alastuey, A., Allan, J. D., Aurela, M., Berico, M., Bougiatioti, A., Bukowiecki, N., Canonaco, F., Crenn, V., Dusanter, S., Ehn, M., Elsasser, M., Flentje, H., M., Flentje, H., Graf, P., Green, D. C., Heikkinen, L., Hermann, H., Holzinger, R., Hueglin, C., Keernik, H., Kiendler-Scharr, A., Kubelova, L., Lunder, C., Maasikmets, M., Makes, O., Malaguti, A., Mihalopoulos, N., Nicolas, J.B., O'Dowd, C., Ovadnevaite, J., Petralia, E., Poulain, L., Priestman, M., Riffault, V., Ripoll, A., Schlag, P., Schwarz, J., Sciarec,, J., Slowik, J., Sosedova, Y., Stavroulas, I., Teinemaa, E., Via, M., Vodickar, P., Williams, P.I., Wiedensohler, A., Young, D.E., Zhang, S., Favez, O., Minguillon, M.C., and Prevot, A. S. H.: A European aerosol phenomenology - 7: High-time resolution chemical characteristics of submicron particulate matter across Europe, Atmos. Environ, X, 10, https://doi.org/10.1016/j.aeaoa.2021.100108, 2021.

728 Canagaratna, M. R., Jayne, J. T., Ghertner, D. A., Herndon, S., Shi, Q., Jimenez, J. L., Silva, P. J., Williams, P., Lanni, T., Drewnick, F., Demerjian, K. L., Kolb, C. E., and Worsnop, D. R.: Chase studies of particulate emissions from in-use New York City vehicles, Aerosol Sci Technol., 38(6), 555–573, https://doi.org/10.1080/02786820490465504, 2004.

732 Canagaratna, M. R., Jimenez, J. L., Kroll, J. H., Chen, Q., Kessler, S. H., Massoli, P., Hildebrandt Ruiz, L., Fortner, E., Williams, L. R., Wilson, K. R., Surratt, J. D., Donahue, N. M., Jayne, J. T., and Worsnop, D. R.: Elemental ratio measurements of organic compounds using aerosol mass spectrometry: Characterization, improved calibration, and implications, Atmos. Chem. Phys., 15(1), 253–272, https://doi.org/10.5194/acp-15-253-2015, 2015.

736 Canonaco, F., Crippa, M., Slowik, J. G., Baltensperger, U., and Prévôt, A. S. H.: SoFi, an IGOR-based interface for the efficient use of the generalized multilinear engine (ME-2) for the source apportionment: ME-2 application to aerosol mass spectrometer data, Atmos. Meas. Tech., 6(12), 3649–3661, https://doi.org/10.5194/amt-6-3649-2013, (2013).

740 Canonaco, F., Slowik, J. G., Baltensperger, U., and Prévôt, A. S. H.: Seasonal differences in oxygenated organic aerosol composition: Implications for emissions sources and factor analysis, Atmos. Chem. Phys., 15(12), 6993–7002, https://doi.org/10.5194/acp-15-6993-2015, 2015.

743 Canonaco, F., Tobler, A., Chen, G., Sosedova, Y., Gates Slowik, J., Bozzetti, C., Rudolf Daellenbach, K., el Haddad, I., Crippa, M., Huang, R. J., Furger, M., Baltensperger, U., and Prévôt, A. S. H.: A new method for long-term source apportionment with time-dependent factor profiles and uncertainty assessment using SoFi Pro: Application to 1 year of organic aerosol data. Atmos. Meas. Tech., 14(2), 923–943, https://doi.org/10.5194/amt-14-923-2021, 2021.

748 Canonaco, F., Tobler, A., Chen, G., Sosedova, Y., Slowik, J. G., Bozzetti, C., Daellenbach, K. R., ElHaddad, I., Crippa, M., Huang, R.-J., Furger, M., Baltensperger, U., and Prévôt, A. S. H.: A new method for long-term source

https://doi.org/10.5194/acp-2022-842
Preprint. Discussion started: 11 January 2023

Atmospheric Chemistry and Physics Discussions

apportionment with time-dependent factor profiles and uncertainty assessment using SoFi Pro: application to one year of organic aerosol data, Atmos. Meas. Tech., 1–39, https://doi.org/10.5194/amt-2020-204, 2020.

Chazeau, B., el Haddad, I., Canonaco, F., Temime-Roussel, B., D'Anna, B., Gille, G., Mesbah, B., Prévôt, A. S. H., Wortham, H., and Marchand, N.: Organic aerosol source apportionment by using rolling positive matrix factorization: Application to a Mediterranean coastal city, Atmos. Environ., X, 14, https://doi.org/10.1016/j.aeaoa.2022.100176, 2022.

Chen, G., Canonaco, F., Tobler, A., Aas, W., Alastuey, A., Allan, J., Atabakhsh, S., Aurela, M., Baltensperger, U., Bougiatioti, A., de Brito, J. F., Ceburnis, D., Chazeau, B., Chebaicheb, H., Daellenbach, K. R., Ehn, M., el Haddad, I., Eleftheriadis, K., Favez, O., Flentje, H., Font, A., Fossum, K., Freney, E., Gini, M., Green, D.C., Heikkinen, L., Herrmann, H., Kalogridis, A., Keernik, H., Lhotka, R., Lin, C., Lunder, C., Maasikmets, M., Manousakas, M.I., Marchand, N., Marin, C., Marmureanu, L., Mihalopoulos, N., Mocnika, G., Nęckia, J., O'Dowd, C., Ovadnevaite, J., Petera, T., Petita, J.E., Pikridasa, M., Matthew Platt, S., Pokorna, P., Poulain, L., Priestman, M., Riffault, V., Rinaldia, M., Rozanskia, K., Schwarz, J., Sciarea, J., Simon, L., Skiba, A., Slowik, J.G., Sosedova, Y., Stavroulas, I., Styszkoa, K., Teinemaa, E., Timonen, H., Tremper, A., Vasilescu, J., Via, M., Vodicka, P., Wiedensohler, A., Zografou, O., Cruz Minguillon, M., and Prévôt, A. S. H.: European aerosol phenomenology − 8: Harmonised source apportionment of organic aerosol using 22 Year-long ACSM/AMS datasets, Environ. Int., 166, https://doi.org/10.1016/j.envint.2022.107325, 2022.

Chen, G., Sosedova, Y., Canonaco, F., Fröhlich, R., Tobler, A., Vlachou, A., Daellenbach, K., Bozzetti, C., Hueglin, C., Graf, P., Baltensperger, U., Slowik, J., el Haddad, I., and Prévôt, A.: Time dependent source apportionment of submicron organic aerosol for a rural site in an alpine valley using a rolling PMF window, Atmos. Chem. Phys., 1–52, https://doi.org/10.5194/acp-2020-1263, 2020.

Chen, G., Sosedova, Y., Canonaco, F., Fröhlich, R., Tobler, A., Vlachou, A., Daellenbach, K. R., Bozzetti, C., Hueglin, C., Graf, P., Baltensperger, U., Slowik, J. G., el Haddad, I., and Prévôt, A. S. H.: Time-dependent source apportionment of submicron organic aerosol for a rural site in an alpine valley using a rolling positive matrix factorisation (PMF) window, Atmos. Chem. Phys., 21(19), 15081–15101, https://doi.org/10.5194/acp-21-15081-2021, 2021.

Crippa, M., Canonaco, F., Lanz, V. A., Äijälä, M., Allan, J. D., Carbone, S., Capes, G., Ceburnis, D., Dall'Osto, M., Day, D. A., DeCarlo, P. F., Ehn, M., Eriksson, A., Freney, E., Ruiz, L. H., Hillamo, R., Jimenez, J. L., Junninen, H., Kiendler-Scharr, A., Kortelainen, A.-M., Kulmala, M., Laaksonen, A., Mensah10, A.A., Mohr1, C., Nemitz, E., O'Dowd, C., Ovadnevaite, J., Pandis, S. N., Petäjä, T., Poulain, L., Saarikoski, S., Sellegri, K., Swietlicki, E., Tiitta, P., Worsnop, D. R., Baltensperger, U., and Prévôt, A. S. H.: Organic aerosol components derived from 25 AMS data sets across Europe using a consistent ME-2 based source apportionment approach. Atmos. Chem. Phys., 14(12), 6159–6176, https://doi.org/10.5194/acp-14-6159-2014, 2014.

https://doi.org/10.5194/acp-2022-842
Preprint. Discussion started: 11 January 2023

783 Crippa, M., Decarlo, P. F., Slowik, J. G., Mohr, C., Heringa, M. F., Chirico, R., Poulain, L., Freutel, F., Sciare, J., Cozic,
784 J., di Marco, C. F., Elsasser, M., Nicolas, J. B., Marchand, N., Abidi, E., Wiedensohler, A., Drewnick, F.,
785 Schneider, J., Borrmann, S., Nemitz, E., Zimmermann, R., Jaffrezo, J.-L., Prevot, A. S. H., and Baltensperger, U.
786 Wintertime aerosol chemical composition and source apportionment of the organic fraction in the metropolitan
787 area of Paris, Atmos. Chem. Phys., 13(2), 961–981, https://doi.org/10.5194/acp-13-961-2013, 2013.
788 Daellenbach, K. R., Uzu, G., Jiang, J., Cassagnes, L. E., Leni, Z., Vlachou, A., Stefenelli, G., Canonaco, F., Weber, S.,
789 Segers, A., Kuenen, J. J. P., Schaap, M., Favez, O., Albinet, A., Aksoyoglu, S., Dommen, J., Baltensperger, U.,
790 Geiser, M., el Haddad, I., Jaffrezo, J.L., and Prévôt, A. S. H.: Sources of particulate-matter air pollution and its
791 oxidative potential in Europe, Nature, 587(7834), 414–419, https://doi.org/10.1038/s41586-020-2902-8, 2020.
792 Dall'Osto, M., Ovadnevaite, J., Ceburnis, D., Martin, D., Healy, R. M., O'Connor, I. P., Kourtchev, I., Sodeau, J. R.,
793 Wenger, J. C., and O'Dowd, C.: Characterization of urban aerosol in Cork city (Ireland) using aerosol mass
794 spectrometry. Atmos. Chem. Phys., 13(9), 4997–5015, https://doi.org/10.5194/acp-13-4997-2013, 2013.
795 Draxler, R.R. and Hess, G.D.: Description of the HYSPLIT-4 Modeling System, NOAA Technical Memorandum ERL
796 ARL-224, NOAA Air Resources Laboratory, Silver Spring, 1-24, 1997.
797 Dudoitis, V., Byčenkiene, S., Plauškaite, K., Bozzetti, C., Fröhlich, R., Mordas, G., and Ulevičius, V.: Spatial
798 distribution of carbonaceous aerosol in the southeastern Baltic Sea region (event of grass fires), Acta Geophysica,
799 64(3), 711–731, https://doi.org/10.1515/acgeo-2016-0018, 2016.
800 Energy statistics - an overview - Statistics Explained, https://ec.europa.eu/eurostat/statistics-
801 explained/index.php?title=Energy_statistics_-_an_overview, 2022.
802 Europe's coal exit - Europe Beyond Coal: Europe Beyond Coal, https://beyond-coal.eu/europes-coal-exit/, 2022.
803 Fröhlich, R., Crenn, V., Setyan, A., Belis, C. A., Canonaco, F., Favez, O., Riffault, V., Slowik, J. G., Aas, W., Aijälä,
804 M., Alastuey, A., Artiñano, B., Bonnaire, N., Bozzetti, C., Bressi, M., Carbone, C., Coz, E., Croteau, P. L.,
805 Cubison, M. J., Esser-Gietl, J. K., Green, D. C., Gros, V., Heikkinen, L., Herrmann, H., Jayne, J. T., Lunder, C.
806 R., Minguillón, M. C., Mocnik, G., O'Dowd, C. D., Ovadnevaite, J., Petralia, E., Poulain, L., Priestman, M., Ripol,
807 Sarda-Estève, A., R., Wiedensohler, A., Baltensperger, U., Sciare, J., and Prévôt, A. S. H., ACTRIS ACSM
808 intercomparison - Part 2: Intercomparison of ME-2 organic source apportionment results from 15 individual, co-
809 located aerosol mass spectrometers, Atmos. Meas. Tech., 8(6), 2555–2576, https://doi.org/10.5194/amt-8-2555-
810 2015, 2015.
811 Fröhlich, R., Cubison, M. J., Slowik, J. G., Bukowiecki, N., Prévôt, A. S. H., Baltensperger, U., Schneider, J., Kimmel,
812 J. R., Gonin, M., Rohner, U., Worsnop, D. R., and Jayne, J. T.: The ToF-ACSM: A portable aerosol chemical
813 speciation monitor with TOFMS detection. Atmos. Meas. Tech., 6(11), 3225–3241, https://doi.org/10.5194/amt-
814 6-3225-2013, 2013.
815 Gilardoni, S., Massoli, P., Paglione, M., Giulianelli, L., Carbone, C., Rinaldi, M., Decesari, S., Sandrini, S., Costabile,
816 F., Gobbi, G. P., Pietrogrande, M. C., Visentin, M., Scotto, F., Fuzzi, S., and Facchini, M. C.: Direct observation

of aqueous secondary organic aerosol from biomass-burning emissions, Proceedings of the National Academy of Sciences of the United States of America, 113(36), 10013–10018, https://doi.org/10.1073/pnas.1602212113, 2016.

Heikkinen, L., Äijälä, M., Daellenbach, K., Chen, G., Garmash, O., Aliaga, D., Graeffe, F., Räty, M., Luoma, K., Aalto, P., Kulmala, M., Petäjä, T., Worsnop, D., and Ehn, M.: Eight years of sub-micrometre organic aerosol composition data from the boreal forest characterized using a machine-learning approach, Atmos. Chem. Phys., 1–47, https://doi.org/10.5194/acp-2020-868, 2020.

Henry, R., Norris, G. A., Vedantham, R., and Turner, J. R.: Source region identification using kernel smoothing, Environ. Sci. Technol., 43(11), 4090–4097, https://doi.org/10.1021/es8011723, 2009.

Huang, S., Wu, Z., Poulain, L., van Pinxteren, M., Merkel, M., Assmann, D., Herrmann, H., and Wiedensohler, A.: Source apportionment of the organic aerosol over the Atlantic Ocean from 53°N to 53°S: Significant contributions from marine emissions and long-range transport, Atmos. Chem. Phys., 18(24), 18043–18062, https://doi.org/10.5194/acp-18-18043-2018, 2018.

Huang, W., Saathoff, H., Shen, X., Ramisetty, R., Leisner, T., and Mohr, C.: Seasonal characteristics of organic aerosol chemical composition and volatility in Stuttgart, Germany, Atmos. Chem. Phys., 19(18), 11687–11700, https://doi.org/10.5194/acp-19-11687-2019, 2019.

Hussein, T., Karppinen, A., Kukkonen, J., Härkönen, J., Aalto, P. P., Hämeri, K., Kerminen, V. M., and Kulmala, M.: Meteorological dependence of size-fractionated number concentrations of urban aerosol particles, Atmos. Environ., 40(8), 1427–1440, https://doi.org/10.1016/j.atmosenv.2005.10.061, 2006.

Iapalucci, T. L., Demski, R. J., and Bienstock, D.: Chlorine in Coal Combustion. United States Department of the Interior, Bureau of Mines Report of Investigation 7260s, 1969.

Iinuma, Y., Engling, G., Puxbaum, H., and Herrmann, H.: A highly resolved anion-exchange chromatographic method for determination of saccharidic tracers for biomass combustion and primary bio-particles in atmospheric aerosol, Atmos. Environ., 43(6), 1367–1371, https://doi.org/10.1016/j.atmosenv.2008.11.020, 2009.

Jayne, J. T., Leard, D. C., Zhang, X., Davidovits, P., Smith, K. A., Kolb, C. E., and Worsnop, D. R.: Development of an Aerosol Mass Spectrometer for Size and Composition Analysis of Submicron Particles, Aerosol Sci Technol., 33:1-2, 48-70, https://doi.org/10.1080/027868200410840, 2000.

Jimenez, J. L., Canagaratna, M. R., Donahue, N. M., Prevot, A. S. H., Zhang, Q., Kroll, J. H., DeCarlo, P. F., Allan, J. D., Coe, H., Ng, N. L., Aiken, A. C., Docherty, K. S., Ulbrich, I. M., Grieshop, A. P., Robinson, A. L., Duplissy, J., Smith, J. D., Wilson, K. R., Lanz, V. A., Hueglin, C., Sun, Y. L., Tian, J., Laaksonen, A., Raatikainen, T., Rautiainen, J., Vaattovaara, P., Ehn, M., Kulmala, M., Tomlinson, J. M., Collins, D. R., Cubison, M. J., Dunlea, E. J., Huffman, J. A., Onasch, T. B., Alfarra, M. R., Williams, P. I., Bower, K., Kondo, Y., Schneider, J., Drewnick, F., Borrmann, S., Weimer, S., Demerjian, K., Salcedo, D., Cottrell, L., Griffin, R., Takami, A., Miyoshi, T., Hatakeyama, S., Shimono, A., Sun, J. Y, Zhang, Y. M., Dzepina, K., Kimmel, J. R., Sueper, D., Jayne, J. T.,

https://doi.org/10.5194/acp-2022-842
Preprint. Discussion started: 11 January 2023

Herndon, S. C., Trimborn, A. M., Williams, L. R., Wood, E. C., Middlebrook, A. M., Kolb, C. E., Baltensperger, U., and Worsnop, D. R.: Evolution of organic aerosols in the atmosphere. Science, 326(5959), 1525–1529, https://doi.org/10.1126/science.1180353, 2009.

Katsanos, D., Bougiatioti, A., Liakakou, E., Kaskaoutis, D. G., Stavroulas, I., Paraskevopoulou, D., Lianou, M., Psiloglou, B. E., Gerasopoulos, E., Pilinis, C., and Mihalopoulos, N.: Optical properties of near-surface urban aerosols and their chemical tracing in a mediterranean city (Athens), Aerosol and Air Quality Research, 19(1), 49–70, https://doi.org/10.4209/aaqr.2017.11.0544, 2019.

Kiendler-Scharr, A., Mensah, A. A., Friese, E., Topping, D., Nemitz, E., Prevot, A. S. H., Äijälä, M., Allan, J., Canonaco, F., Canagaratna, M., Carbone, S., Crippa, M., Dall Osto, M., Day, D. A., de Carlo, P., di Marco, C. F., Elbern, H., Eriksson, A., Freney, E., Hao, L., Herrmann, H., Hildebrandt, L.,. Hillamo, R., Jimenez, J. L., Laaksonen, A., McFiggans, G., Mohr, C., O'Dowd, C., Otjes, R., Ovadnevaite, J., Pandis, S. N., Poulain, L., Schlag, P., Sellegri, K., Swietlicki, E., Tiitta, P., Vermeulen, A., Wahner, A., Worsnop, D. and Wu, H. C.: Ubiquity of organic nitrates from night time chemistry in the European submicron aerosol, Geophysical Research Letters, 43(14), 7735–7744, https://doi.org/10.1002/2016GL069239, 2016.

Kumar, V., Giannoukos, S., Haslett, S. L., Tong, Y., Singh, A., Bertrand, A., Lee, C. P., Wang, D. S., Bhattu, D., Stefenelli, G., Dave, J. S., Puthussery, J. v., Qi, L., Vats, P., Rai, P., Casotto, R., Satish, R., Mishra, S., Pospisilova, V., C., Bell, D.M., Ganguly, D., Verma, V., Rastogi, N., Baltensperger, U., Tripathi, S.N., Prévôt, A.S.H., and Slowik, J. G.: Highly time-resolved chemical speciation and source apportionment of organic aerosol components in Delhi, India, using extractive electrospray ionization mass spectrometry, Atmos. Chem. Phys., 22(11), 7739–7761, https://doi.org/10.5194/acp-22-7739-2022, 2022.

Laborde, M., Crippa, M., Tritscher, T., Jurányi, Z., Decarlo, P. F., Temime-Roussel, B., Marchand, N., Eckhardt, S., Stohl, A., Baltensperger, U., Prévôt, A. S. H., Weingartner, E., and Gysel, M.: Black carbon physical properties and mixing state in the European megacity Paris, Atmos. Chem. Phys., 13(11), 5831–5856, https://doi.org/10.5194/acp-13-5831-2013, 2013.

Lanz, V. A., Alfarra, M. R., Baltensperger, U., Buchmann, B., Hueglin, C., and Prévôt, A. S. H.: Source apportionment of submicron organic aerosols at an urban site by factor analytical modelling of aerosol mass spectra, Atmos. Chem. Phys., 7, www.atmos-chem-phys.net/7/1503/2007/, 2007.

Lanz, V. A., Alfarra, M. R., Baltensperger, U., Buchmann, B., Hueglin, C., Szidat, S., Wehrli, M. N., Wacker, L., Weimer, S., Caseiro, A., Puxbaum, H., and Prevot, A. S. H.: Source attribution of submicron organic aerosols during wintertime inversions by advanced factor analysis of aerosol mass spectra, Environ. Sci. Technol., 42(1), 214–220, https://doi.org/10.1021/es0707207, 2008.

Li, G., Lei, W., Bei, N., and Molina, L. T.: Contribution of garbage burning to chloride and PM 2.5 in Mexico City, Atmos. Chem. Phys., 12(18), 8751–8761, https://doi.org/10.5194/acp-12-8751-2012, 2012.

884 Lin, C., Ceburnis, D., Hellebust, S., Buckley, P., Wenger, J., Canonaco, F., Prévôt, A. S. H., Huang, R. J., O'Dowd, C.,
885 and Ovadnevaite, J.: Characterization of Primary Organic Aerosol from Domestic Wood, Peat, and Coal Burning
886 in Ireland, Environ. Sci. Technol., 51(18), 10624–10632, https://doi.org/10.1021/acs.est.7b01926, 2017.
887 Liu, P. S. K., Deng, R., Smith, K. A., Williams, L. R., Jayne, J. T., Canagaratna, M. R., Moore, K., Onasch, T. B.,
888 Worsnop, D. R., and Deshler, T.: Transmission efficiency of an aerodynamic focusing lens system: Comparison
889 of model calculations and laboratory measurements for the aerodyne aerosol mass spectrometer, Aerosol Sci
890 Technol., 41(8), 721–733, https://doi.org/10.1080/02786820701422278, 2007.
891 Ma, N., Birmili, W., Müller, T., Tuch, T., Cheng, Y. F., Xu, W. Y., Zhao, C. S., and Wiedensohler, A.: Tropospheric
892 aerosol scattering and absorption over central Europe: A closure study for the dry particle state. Atmos. Chem.
893 Phys., 14(12), 6241–6259, https://doi.org/10.5194/acp-14-6241-2014, 2014.
894 Middlebrook, A. M., Bahreini, R., Jimenez, J. L., and Canagaratna, M. R.: Evaluation of composition-dependent
895 collection efficiencies for the Aerodyne aerosol mass spectrometer using field data. Aerosol Sci Technol., 46(3),
896 258–271, https://doi.org/10.1080/02786826.2011.620041, 2012.
897 Ng, N. L., Canagaratna, M. R., Zhang, Q., Jimenez, J. L., Tian, J., Ulbrich, I. M., Kroll, J. H., Docherty, K. S., Chhabra,
898 P. S., Bahreini, R., Murphy, S. M., Seinfeld, J. H., Hildebrandt, L., Donahue, N. M., Decarlo, P. F., Lanz, V. A.,
899 Prévôt, A. S. H., Dinar, E., Rudich, Y., and Worsnop, D. R.: Organic aerosol components observed in Northern
900 Hemispheric datasets from Aerosol Mass Spectrometry, Atmos. Chem. Phys., 10(10), 4625–4641,
901 https://doi.org/10.5194/acp-10-4625-2010, 2010.
902 Ng, N. L., Herndon, S. C., Trimborn, A., Canagaratna, M. R., Croteau, P. L., Onasch, T. B., Sueper, D., Worsnop, D.
903 R., Zhang, Q., Sun, Y. L., and Jayne, J. T.: An Aerosol Chemical Speciation Monitor (ACSM) for routine
904 monitoring of the composition and mass concentrations of ambient aerosol, Aerosol Sci Technol., 45(7), 780–
905 794, https://doi.org/10.1080/02786826.2011.560211, 2011.
906 O'Dowd, C., Ceburnis, D., Ovadnevaite, J., Vaishya, A., Rinaldi, M., and Facchini, M. C.: Do anthropogenic,
907 continental or coastal aerosol sources impact on a marine aerosol signature at Mace Head? Atmos. Chem. Phys.,
908 14(19), 10687–10704, https://doi.org/10.5194/acp-14-10687-2014, 2014.
909 Ovadnevaite, J., Ceburnis, D., Leinert, S., Dall'Osto, M., Canagaratna, M., O'Doherty, S., Berresheim, H., and O'Dowd,
910 C.: Submicron NE Atlantic marine aerosol chemical composition and abundance: Seasonal trends and air mass
911 categorization, J. Geophys. Res., 119(20), 11,850-11,863, https://doi.org/10.1002/2013JD021330, 2014.
912 Paatero, P.: Least squares formulation of robust non-negative factor analysis, In Chemometrics and Intelligent
913 Laboratory Systems, 37, 1997.
914 Paatero, P.: The Multilinear Engine- A Table-Driven, Least Squares Program for Solving Multilinear Problems,
915 Including the n-Way Parallel Factor Analysis Model, J Comput Graph Stat., 8(4), 854–888,
916 https://doi.org/10.1080/10618600.1999.10474853, 1999.

Paatero, P., and Tappert, U.: Positive matrix factorization: A non-negative factor model with optimal utilization of error estimates of data values *, ENVIRONMETRICS, 5, 111-126, 1994.

Paglione, M., Gilardoni, S., Rinaldi, M., Decesari, S., Zanca, N., Sandrini, S., Giulianelli, L., Bacco, D., Ferrari, S., Poluzzi, V., Scotto, F., Trentini, A., Poulain, L., Herrmann, H., Wiedensohler, A., Canonaco, F., Prévôt, A. S. H., Massoli, P., Carbone, C., C., Bell, D.M., Ganguly, D., Verma, V., Rastogi, N., Baltensperger, U., Tripathi, S.N., Prévôt, A.S.H., and Fuzzi, S.: The impact of biomass burning and aqueous-phase processing on air quality: A multi-year source apportionment study in the Po Valley, Italy, Atmos. Chem. Phys., 20(3), 1233–1254, https://doi.org/10.5194/acp-20-1233-2020, 2020.

Parworth, C., Fast, J., Mei, F., Shippert, T., Sivaraman, C., Tilp, A., Watson, T., and Zhang, Q.: Long-term measurements of submicrometer aerosol chemistry at the Southern Great Plains (SGP) using an Aerosol Chemical Speciation Monitor (ACSM), Atmos. Environ., 106, 43–55, https://doi.org/10.1016/j.atmosenv.2015.01.060, 2015.

Petit, J.-E., Favez, O., Sciare, J., Crenn, V., Sarda-Esteve, R., Bonnaire, N., Mocnik, G., Dupont, J. C., Haeffelin, M., Leoz-Garziandia, E., Sarda, R., Petit, J.-E., Favez, O., Sciare, J., Crenn, V., Sarda-Estève, R., Bonnaire, N., Močnik, G., Dupont, J.-C., Haeffelin., M., and Leoz-Garziandia, E.: Two years of near real-time chemical composition of submicron aerosols in the region of Paris using an Aerosol Chemical Speciation Monitor (ACSM) and a multi-wavelength Aethalometer, European Geosciences Union, 15(6), 2985–3005, https://doi.org/10.5194/acpd-14-24221-2014ï, 2015.

Petzold, A., and Schönlinner, M.: Multi-angle absorption photometry - A new method for the measurement of aerosol light absorption and atmospheric black carbon, J. Aerosol Sci., 35(4), 421–441, https://doi.org/10.1016/j.jaerosci.2003.09.005, 2004.

Poulain, L., Birmili, W., Canonaco, F., Crippa, M., Wu, Z. J., Nordmann, S., Spindler, G., Prévôt, A. S. H., Wiedensohler, A., and Herrmann, H.: Chemical mass balance of 300 °c non-volatile particles at the tropospheric research site Melpitz, Germany, Atmos. Chem. Phys., 14(18), 10145–10162, https://doi.org/10.5194/acp-14-10145-2014, 2014.

Poulain, L., Fahlbusch, B., Spindler, G., Müller, K., van Pinxteren, D., Wu, Z., Iinuma, Y., Birmili, W., Wiedensohler, A., and Herrmann, H.: Source apportionment and impact of long-range transport on carbonaceous aerosol particles in Central Germany during HCCT-2010, Atmos. Chem. Phys., 1–33, https://doi.org/10.5194/acp-2020-626, 2020.

Poulain, L., Fahlbusch, B., Spindler, G., Müller, K., van Pinxteren, D., Wu, Z., Iinuma, Y., Birmili, W., Wiedensohler, A., and Herrmann, H.: Source apportionment and impact of long-range transport on carbonaceous aerosol particles in central Germany during HCCT-2010, Atmos. Chem. Phys., 21(5), 3667–3684, https://doi.org/10.5194/acp-21-3667-2021, 2021.

Poulain, L., Spindler, G., Birmili, W., Plass-Dülmer, C., Wiedensohler, A., and Herrmann, H.: Seasonal and diurnal variations of particulate nitrate and organic matter at the IfT research station Melpitz. Atmos. Chem. Phys., 11(24), 12579–12599, https://doi.org/10.5194/acp-11-12579-2011, 2011.

Poulain, L., Spindler, G., Grüner, A., Tuch, T., Stieger, B., Pinxteren, D. van, Petit, J. E., Favez, O., Herrmann, H., and Wiedensohler, A.: Multi-year ACSM measurements at the central European research station Melpitz (Germany)-Part 1: Instrument robustness, quality assurance, and impact of upper size cutoff diameter, Atmos. Meas. Tech., 13(9), 4973–4994, https://doi.org/10.5194/amt-13-4973-2020, 2020.

Qi, L., Vogel, A. L., Esmaeilirad, S., Cao, L., Zheng, J., Jaffrezo, J. L., Fermo, P., Kasper-Giebl, A., Daellenbach, K. R., Chen, M., Ge, X., Baltensperger, U., Prévôt, A. S. H., and Slowik, J. G.: A 1-year characterization of organic aerosol composition and sources using an extractive electrospray ionization time-of-flight mass spectrometer (EESI-TOF), Atmos. Chem. Phys., 20(13), 7875–7893, https://doi.org/10.5194/acp-20-7875-2020, 2020.

Schlag, P., Kiendler-Scharr, A., Johannes Blom, M., Canonaco, F., Sebastiaan Henzing, J., Moerman, M., Prévôt, A. S. H., and Holzinger, R.: Aerosol source apportionment from 1-year measurements at the CESAR tower in Cabauw, the Netherlands, Atmos. Chem. Phys., 16(14), 8831–8847, https://doi.org/10.5194/acp-16-8831-2016, 2016.

Seinfeld, J. H., and Pandis, S. N.: Atmospheric Chemistry and Physics: From Air Pollution to Climate Change, 3rd Edition, 1152, ISBN 9781118947401, 2006.

Shi, Y., Chen, J., Hu, D., Wang, L., Yang, X., and Wang, X.: Airborne submicron particulate (PM1) pollution in Shanghai, China: Chemical variability, formation/dissociation of associated semi-volatile components and the impacts on visibility, Science of the Total Environment, 473–474, 199–206, https://doi.org/10.1016/j.scitotenv.2013.12.024, 2014.

Shrivastava, M., Cappa, C. D., Fan, J., Goldstein, A. H., Guenther, A. B., Jimenez, J. L., Kuang, C., Laskin, A., Martin, S. T., Ng, N. L., Petaja, T., Pierce, J. R., Rasch, P. J., Roldin, P., Seinfeld, J. H., Shilling, J., Smith, J. N., Thornton, J. A., Volkamer, R., Wang, J., Worsnop, D.R., Zaveri, R.A., Zelenyuk, A., and Zhang, Q.: Recent advances in understanding secondary organic aerosol: Implications for global climate forcing, Reviews of Geophysics, 55(2), 509–559, https://doi.org/10.1002/2016RG000540, 2017.

Simoneit, B. R. T., and Elias, V. O.: Detecting Organic Tracers from Biomass Burning in the Atmosphere, Marine Pollution Bulletin, 42, 10, 805-810, DOI: 10.1016/s0025-326x(01)00094-7, 2001.

Simoneit, B. R. T., Schauer, J. J., Nolte, C. G., Oros, D. R., Elias, V. O., Fraser, M. P., Rogge, W. F., and Cass, G. R.: Levoglucosan, a tracer for cellulose in biomass burning and atmospheric particles, Atmos. Environ., 33, 173-182, https://doi.org/10.1016/S1352-2310(98)00145-9, 1999.

Spindler, G., Brüggemann, E., Gnauk, T., Grüner, A., Müller, K., and Herrmann, H.: A four-year size-segregated characterization study of particles PM10, PM2.5 and PM1 depending on air mass origin at Melpitz, Atmos. Environ., 44(2), 164–173, https://doi.org/10.1016/j.atmosenv.2009.10.015, 2010.

982 Spindler, G., Gnauk, T., Grüner, A., Iinuma, Y., Müller, K., Scheinhardt, S., and Herrmann, H.: Size-segregated
983 characterization of PM10 at the EMEP site Melpitz (Germany) using a five-stage impactor: A six-year study, J.
984 Atmos. Chem., 69(2), 127–157, https://doi.org/10.1007/s10874-012-9233-6, 2012.
985 Spindler, G., Grüner, A., Müller, K., Schlimper, S., and Herrmann, H.: Long-term size-segregated particle (PM10,
986 PM2.5, PM1) characterization study at Melpitz - Influence of air mass inflow, weather conditions and season, J.
987 Atmos. Chem., 70(2), 165–195, https://doi.org/10.1007/s10874-013-9263-8, 2013.
988 Spindler, G., Müller, K., Brüggemann, E., Gnauk, T., and Herrmann, H.: Long-term size-segregated characterization of
989 PM 10, PM 2.5, and PM_1 at the IfT research station Melpitz downwind of Leipzig (Germany) using high and low-
990 volume filter samplers, Atmos. Environ., 38(31), 5333–5347, https://doi.org/10.1016/j.atmosenv.2003.12.047,
991 2004.
992 Stavroulas, I., Bougiatioti, A., Grivas, G., Paraskevopoulou, D., Tsagkaraki, M., Zarmpas, P., Liakakou, E.,
993 Gerasopoulos, E., and Mihalopoulos, N.K: Sources and processes that control the submicron organic aerosol
994 composition in an urban Mediterranean environment (Athens): A high temporal-resolution chemical composition
995 measurement study, Atmos. Chem. Phys., 19(2), 901–919, https://doi.org/10.5194/acp-19-901-2019, 2019.
996 Stieger, B., Spindler, G., Fahlbusch, B., Müller, K., Grüner, A., Poulain, L., Thöni, L., Seitler, E., Wallasch, M., and
997 Herrmann, H.: Measurements of PM10 ions and trace gases with the online system MARGA at the research station
998 Melpitz in Germany – A five-year study, J. Atmos. Chem., 75(1), 33–70, https://doi.org/10.1007/s10874-017-
999 9361-0, 2018.
1000 Sun, J., Birmili, W., Hermann, M., Tuch, T., Weinhold, K., Merkel, M., Rasch, F., Müller, T., Schladitz, A., Bastian,
1001 S., Löschau, G., Cyrys, J., Gu, J., Flentje, H., Briel, B., Asbach, C., Kaminski, H., Ries, L., Sohmer, R., Gerwig,
1002 H., Wirtz, K., Meinhardt, F., Schwerin, A., Bath, O., Ma, N., and Wiedensohler, A.: Decreasing trends of particle
1003 number and black carbon mass concentrations at 16 observational sites in Germany from 2009 to 2018, Atmos.
1004 Chem. Phys., 20(11), 7049–7068, https://doi.org/10.5194/acp-20-7049-2020, 2020.
1005 Sun, Y., Xu, W., Zhang, Q., Jiang, Q., Canonaco, F., Prévôt, A. S. H., Fu, P., Li, J., Jayne, J., Worsnop, D. R., and
1006 Wang, Z.: Source apportionment of organic aerosol from 2-year highly time-resolved measurements by an aerosol
1007 chemical speciation monitor in Beijing, China, Atmos. Chem. Phys., 18(12), 8469–8489,
1008 https://doi.org/10.5194/acp-18-8469-2018, 2018.
1009 Tiitta, P., Leskinen, A., Hao, L., Yli-Pirilä, P., Kortelainen, M., Grigonyte, J., Tissari, J., Lamberg, H., Hartikainen, A.,
1010 Kuuspalo, K., Kortelainen, A. M., Virtanen, A., Lehtinen, K. E. J., Komppula, M., Pieber, S., Prévôt, A. S. H.,
1011 Onasch, T. B., Worsnop, D. R., Czech, H., Zimmermann, R., Jokiniemi, J., and Sippula, O.: Transformation of
1012 logwood combustion emissions in a smog chamber: Formation of secondary organic aerosol and changes in the
1013 primary organic aerosol upon daytime and night time aging, Atmos. Chem. Phys., 16(20), 13251–13269,
1014 https://doi.org/10.5194/acp-16-13251-2016, 2016.

1015 Tobler, A., Skiba, A., Canonaco, F., Močnik, G., Rai, P., Chen, G., Bartyzel, J., Zimnoch, M., Styszko, K., Nęcki, J.,
1016 Furger, M., Różański, K., Baltensperger, U., Slowik, J., and Prévôt, A.: Characterization of NR-PM1 and source
1017 apportionment of organic aerosol in Krakow, Poland, Atmos. Chem. Phys., 1–22, https://doi.org/10.5194/acp-
1018 2021-197, 2021.
1019 Ulbrich, I. M., Canagaratna, M. R., Zhang, Q., Worsnop, D. R., and Jimenez, J. L.: Interpretation of organic components
1020 from Positive Matrix Factorization of aerosol mass spectrometric data, Atmos. Chem. Phys., 9, www.atmos-chem-
1021 phys.net/9/2891/2009/, 2009.
1022 van Pinxteren, D., Fomba, K. W., Spindler, G., Müller, K., Poulain, L., Iinuma, Y., Löschau, G., Hausmann, A., and
1023 Herrmann, H.; Regional air quality in Leipzig, Germany: Detailed source apportionment of size-resolved aerosol
1024 particles and comparison with the year 2000, Faraday Discussions, 189, 291–315,
1025 https://doi.org/10.1039/c5fd00228a, 2016.
1026 van Pinxteren, D., Engelhardt, V., Mothes, F., Poulain, L., Spindler, G., Cuesta, A., Tuch, T., Müller, T., Wiedensohler,
1027 A., and Herrmann, H.: Residential wood combustion in Germany: A twin-site study of local village contributions
1028 to particulate pollutants, in preparation 2023.
1029 Via, M., Minguillón, M. C., Reche, C., Querol, X., and Alastuey, A.: Increase of secondary organic aerosol over four
1030 years in an urban environment, Atmos. Chem. Phys., 1–20, https://doi.org/10.5194/acp-2020-1244, 2020.
1031 Vlachou, A., Daellenbach, K., Bozzetti, C., Chazeau, B., Salazar, G., Szidat, S., Jaffrezo, J.-L., Hueglin, C.,
1032 Baltensperger, U., Haddad, I. el, Daellenbach, K. R., Salazar, G. A., and Prévôt, A. S. H.: Advanced source
1033 apportionment of carbonaceous aerosols by coupling offline AMS and radiocarbon size-segregated measurements
1034 over a nearly 2-year period, Atmos. Chem. Phys., 18(9), 6187–6206, https://doi.org/10.5194/acp-18-6187-2018ï,
1035 2018.
1036 Vlachou, A., Tobler, A., Lamkaddam, H., Canonaco, F., Daellenbach, K. R., Jaffrezo, J. L., Minguillón, M. C.,
1037 Maasikmets, M., Teinemaa, E., Baltensperger, U., el Haddad, I., and Preávôt, A. S. H.: Development of a versatile
1038 source apportionment analysis based on positive matrix factorization: a case study of the seasonal variation of
1039 organic aerosol sources in Estonia, Atmos. Chem. Phys., 19(11), 7279–7295, https://doi.org/10.5194/acp-19-
1040 7279-2019, 2019.
1041 Wang, T., Fu, T., Chen, K., Cheng, R., Chen, S., Liu, J., Mei, M., Li, J., and Xue, Y.: Co-combustion behavior of dyeing
1042 sludge and rice husk by using TG-MS: Thermal conversion, gas evolution, and kinetic analyses, Bioresource
1043 Technology, 311, https://doi.org/10.1016/j.biortech.2020.123527, 2020.
1044 Wehner, B., Philippin, S., and Wiedensohler, A.: Design and calibration of a thermodenuder with an improved heating
1045 unit to measure the size-dependent volatile fraction of aerosol particles, Aerosol Science, 33,
1046 www.elsevier.com/locate/jaerosci, 2002.

WHO, Expert Consultation: https://www.who.int/news-room/events/detail/2019/02/12/default-calendar/expert-consultation-risk-communication-and-intervention-to-reduce-exposure-and-to-minimize-the-health-effects-of-air-pollution, 2019.

Wierońska-Wiśniewska, F., Makowska, D., and Strugała, A.: Arsenic in polish coals: Content, mode of occurrence, and distribution during coal combustion process, Fuel, 312, https://doi.org/10.1016/j.fuel.2021.122992, 2022.

Xu, W., He, Y., Qiu, Y., Chen, C., Xie, C., Lei, L., Li, Z., Sun, J., Li, J., Fu, P., Wang, Z., Worsnop, D. R., and Sun, Y.: Mass spectral characterization of primary emissions and implications in source apportionment of organic aerosol, Atmos. Meas. Tech., 13(6), 3205–3219, https://doi.org/10.5194/amt-13-3205-2020, 2020.

Yuan, J., Lewis Modini, R., Zanatta, M., Herber, A. B., Müller, T., Wehner, B., Poulain, L., Tuch, T., Baltensperger, U., and Gysel-Beer, M.: Variability in the mass absorption cross section of black carbon (BC) aerosols is driven by BC internal mixing state at a central European background site (Melpitz, Germany) in winter, Atmos. Chem. Phys., 21(2), 635–655, https://doi.org/10.5194/acp-21-635-2021, 2021.

Yudovich, Y. E., and Ketris, M. P.: Chlorine in coal: A review, In International Journal of Coal Geology, 67, Issues 1–2, pp. 127–144, https://doi.org/10.1016/j.coal.2005.09.004, 2006.

Zhang, Q., Jimenez, J. L., Canagaratna, M. R., Ulbrich, I. M., Ng, N. L., Worsnop, D. R., and Sun, Y.: Understanding atmospheric organic aerosols via factor analysis of aerosol mass spectrometry: A review, In Analytical and Bioanalytical Chemistry, 401, Issue 10, pp. 3045–3067, https://doi.org/10.1007/s00216-011-5355-y, 2011.

Zhang, Q., Rami Alfarra, M., Worsnop, D. R., Allan, J. D., Coe, H., Canagaratna, M. R., and Jimenez, J. L.: Deconvolution and quantification of hydrocarbon-like and oxygenated organic aerosols based on aerosol mass spectrometry, Environ. Sci. Technol., 39(13), 4938–4952, https://doi.org/10.1021/es048568l, 2005.

Zhang, Y., Favez, O., Petit, J. E., Canonaco, F., Truong, F., Bonnaire, N., Crenn, V., Amodeo, T., Prévôt, A. S. H., Sciare, J., Gros, V., and Albinet, A.: Six-year source apportionment of submicron organic aerosols from near-continuous highly time-resolved measurements at SIRTA (Paris area, France), Atmos. Chem. Phys., 19(23), 14755–14776, https://doi.org/10.5194/acp-19-14755-2019, 2019.

Zhang, Y. J., Tang, L. L., Wang, Z., Yu, H. X., Sun, Y. L., Liu, D., Qin, W., Canonaco, F., Prévôt, A. S. H., Zhang, H. L., and Zhou, H. C.: Insights into characteristics, sources, and evolution of submicron aerosols during harvest seasons in the Yangtze River delta region, China, Atmos. Chem. Phys., 15(3), 1331–1349, https://doi.org/10.5194/acp-15-1331-2015, 2015.

Zhu, Q., Huang, X. F., Cao, L. M., Wei, L. T., Zhang, B., He, L. Y., Elser, M., Canonaco, F., Slowik, J. G., Bozzetti, C., El-Haddad, I., and Prévôt, A. S. H.: Improved source apportionment of organic aerosols in complex urban air pollution using the multilinear engine (ME-2), Atmos. Meas. Tech., 11(2), 1049–1060, https://doi.org/10.5194/amt-11-1049-2018, 2018.

https://doi.org/10.5194/acp-2022-842
Preprint. Discussion started: 11 January 2023

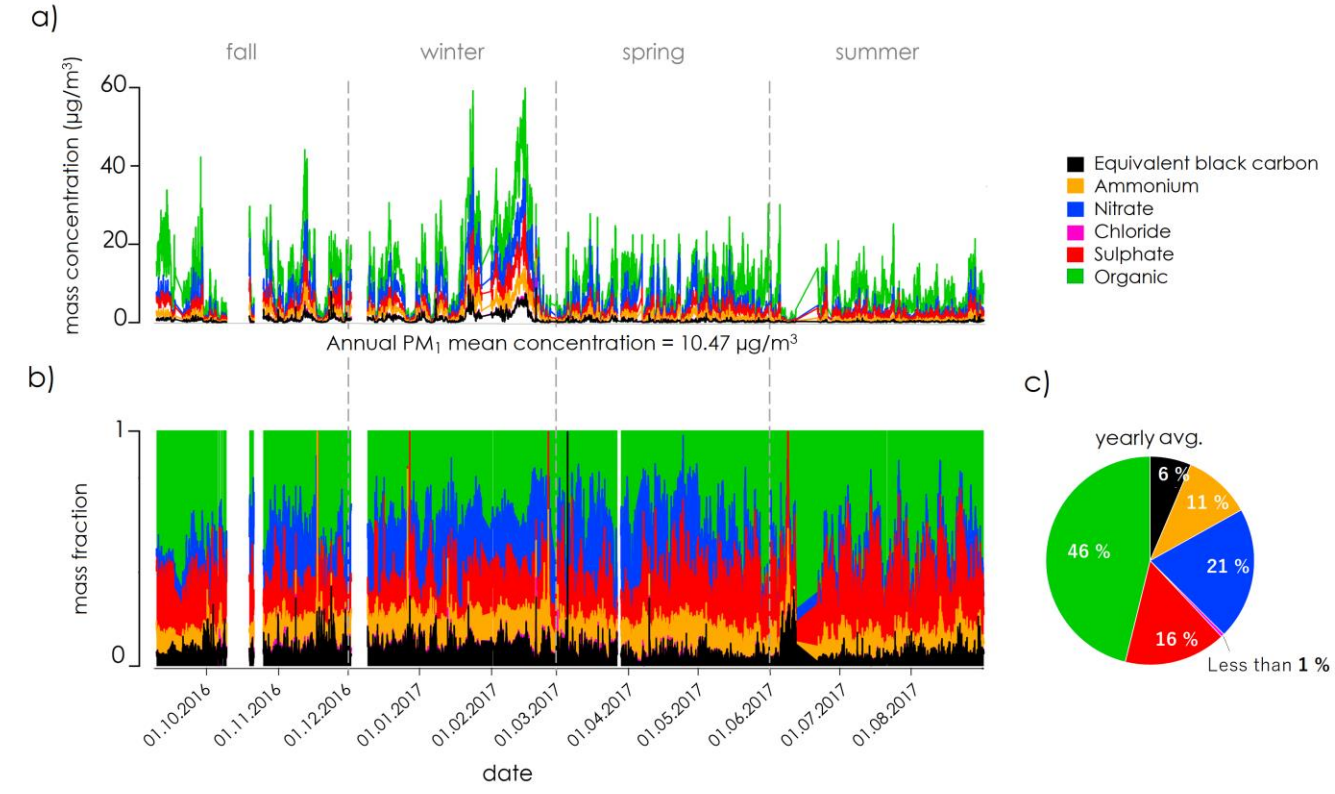

Fig. 1: Time series of a) the particulate PM_1 chemical composition, b) the corresponding mass fraction and c) average contribution of each chemical component (Time is in UTC).

https://doi.org/10.5194/acp-2022-842
Preprint. Discussion started: 11 January 2023

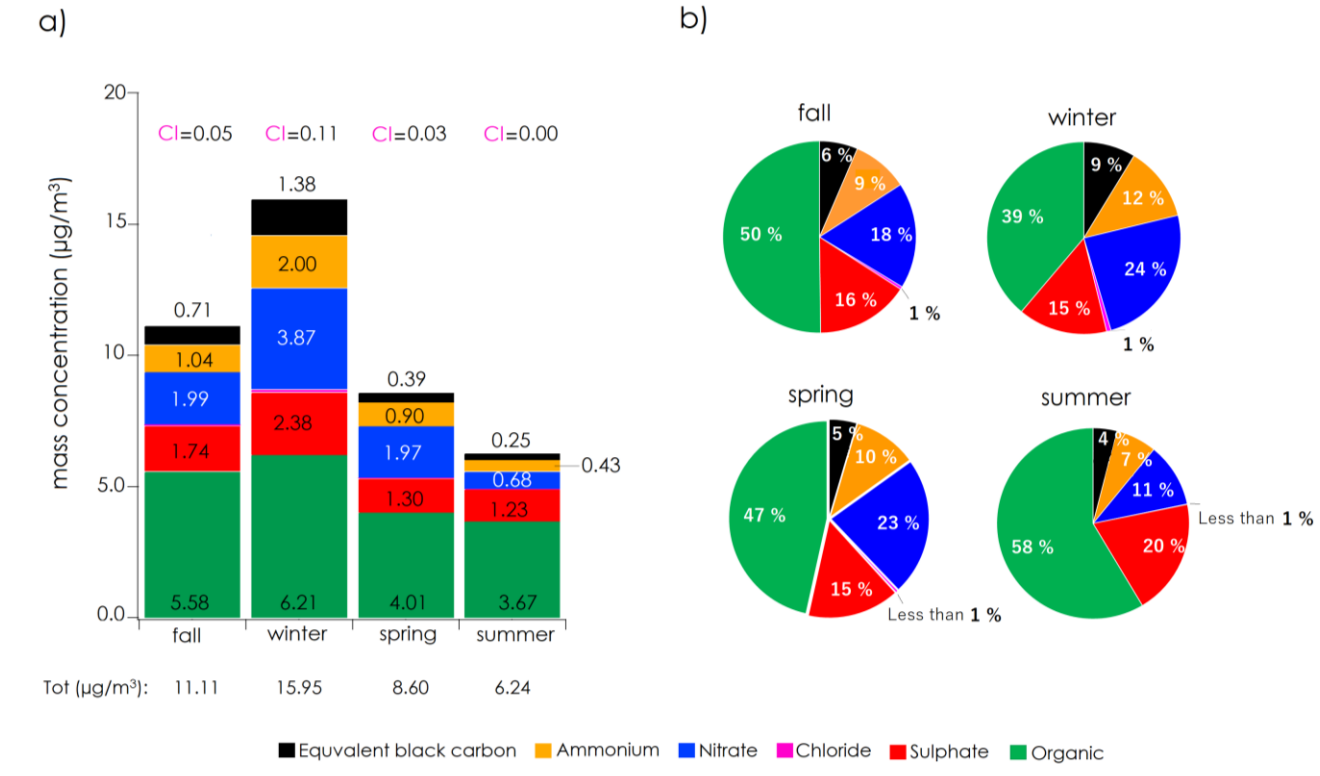

Fig. 2: seasonal variation of PM_1 a) absolute mass concentration and b) mass fraction.

https://doi.org/10.5194/acp-2022-842
Preprint. Discussion started: 11 January 2023

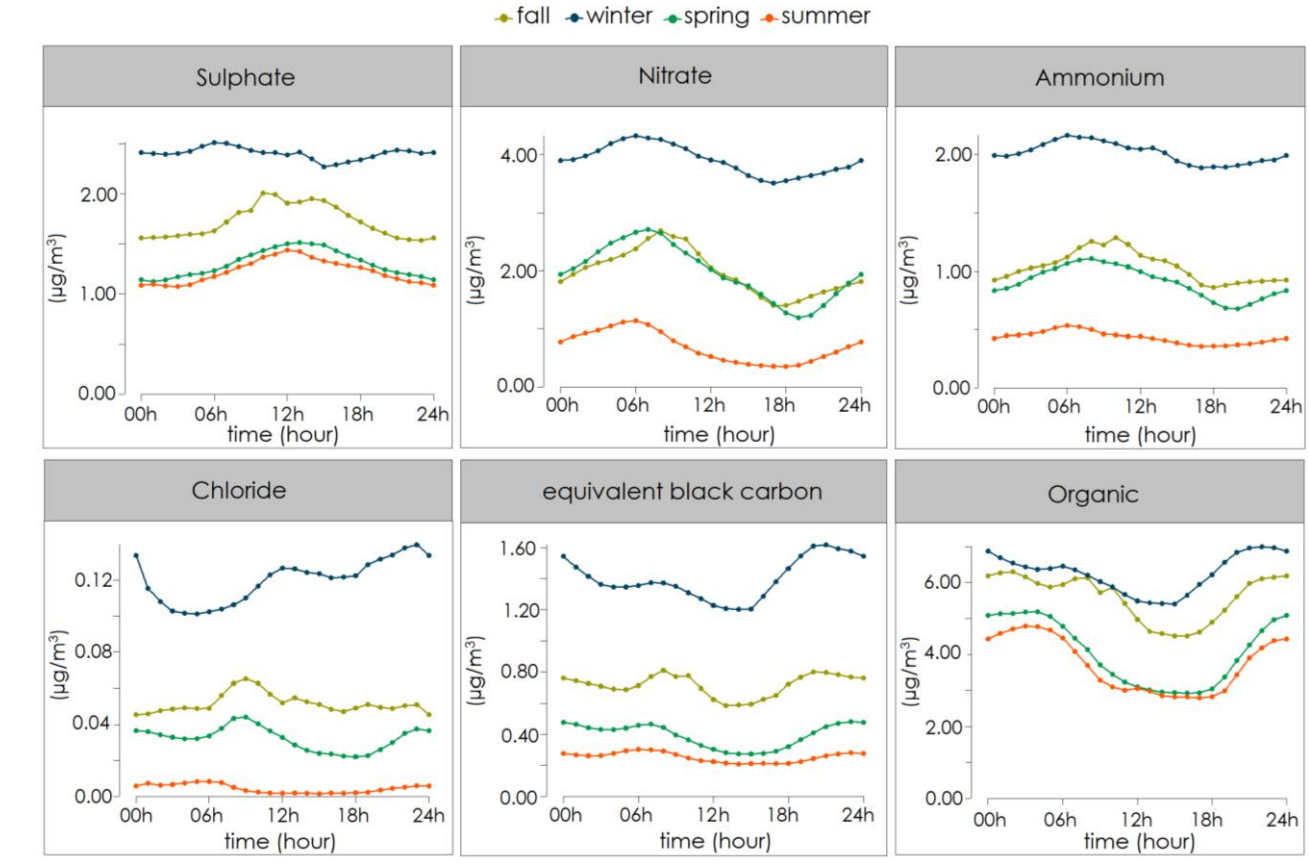

Fig. 3: Seasonal diurnal cycle of PM_1 for ACSM organic and inorganic species (Time is in UTC).

Table. 1: Seasonal/yearly mass concentration of each ACSM species, each PMF factors, contribution of the different POA-PMF-eBC, and correlation of each factors with related species; PM_1.

Species/ Factors		Fall	Winter	Spring	Summer	Yearly
ACSM (µg/m³)	Org	5.58	6.21	4.01	3.67	4.84
	SO_4^{2-}	1.74	2.38	1.30	1.23	1.67
	NO_3^-	1.99	3.87	1.97	0.68	2.16
	NH_4^+	1.04	2.00	0.90	0.43	1.11
	Cl^-	0.05	0.11	0.03	0.00	0.05
MAAP (µg/m³)	eBC	0.71	1.38	0.39	0.25	0.66
PMF (µg/m³)	HOA	0.35	0.36	0.27	0.23	0.30
	BBOA	0.36	0.72	0.27	0.21	0.39
	CCOA	0.72	1.58	0.47	0.30	0.77
	LO-OOA	2.13	1.95	1.24	1.26	1.62
	MO-OOA	2.21	2.25	1.82	1.44	1.92
eBC (µg/m³)	eBC-HOA	0.16	0.19	0.03	0.04	0.05
	eBC-BBOA	0.34	0.38	0.17	0.15	0.25
	eBC-CCOA	0.23	0.74	0.16	0.02	0.37
eBC (%)	eBC-HOA	22	15	9	18	8
	eBC-BBOA	47	29	47	69	37
	eBC-CCOA	31	56	44	13	55

https://doi.org/10.5194/acp-2022-842
Preprint. Discussion started: 11 January 2023

Atmospheric Chemistry and Physics Discussions

Correlation (R^2)	**HOA/eBC**	0.49	0.52	0.34	0.24	0.33
	HOA/NO_x	0.23	0.12	0.32	0.23	0.17
	BBOA/Levo.	0.19	0.59	0.09	0.07	0.54
	BBOA/eBC	0.62	0.81	0.48	0.42	0.77
	CCOA/eBC	0.65	0.85	0.49	0.30	0.82
	CCOA/Cl^-	0.40	0.41	0.18	0.15	0.46
	LO-OOA/ NO_3^-	0.22	0.59	0.01	0.12	0.19
	LO-OOA/ SO_4^2	0.36	0.55	0.00	0.02	0.23
	MO-OOA / SO_4^2	0.58	0.47	0.34	0.42	0.44
	MO-OOA/ NO_3^-	0.24	0.47	0.16	0.24	0.31

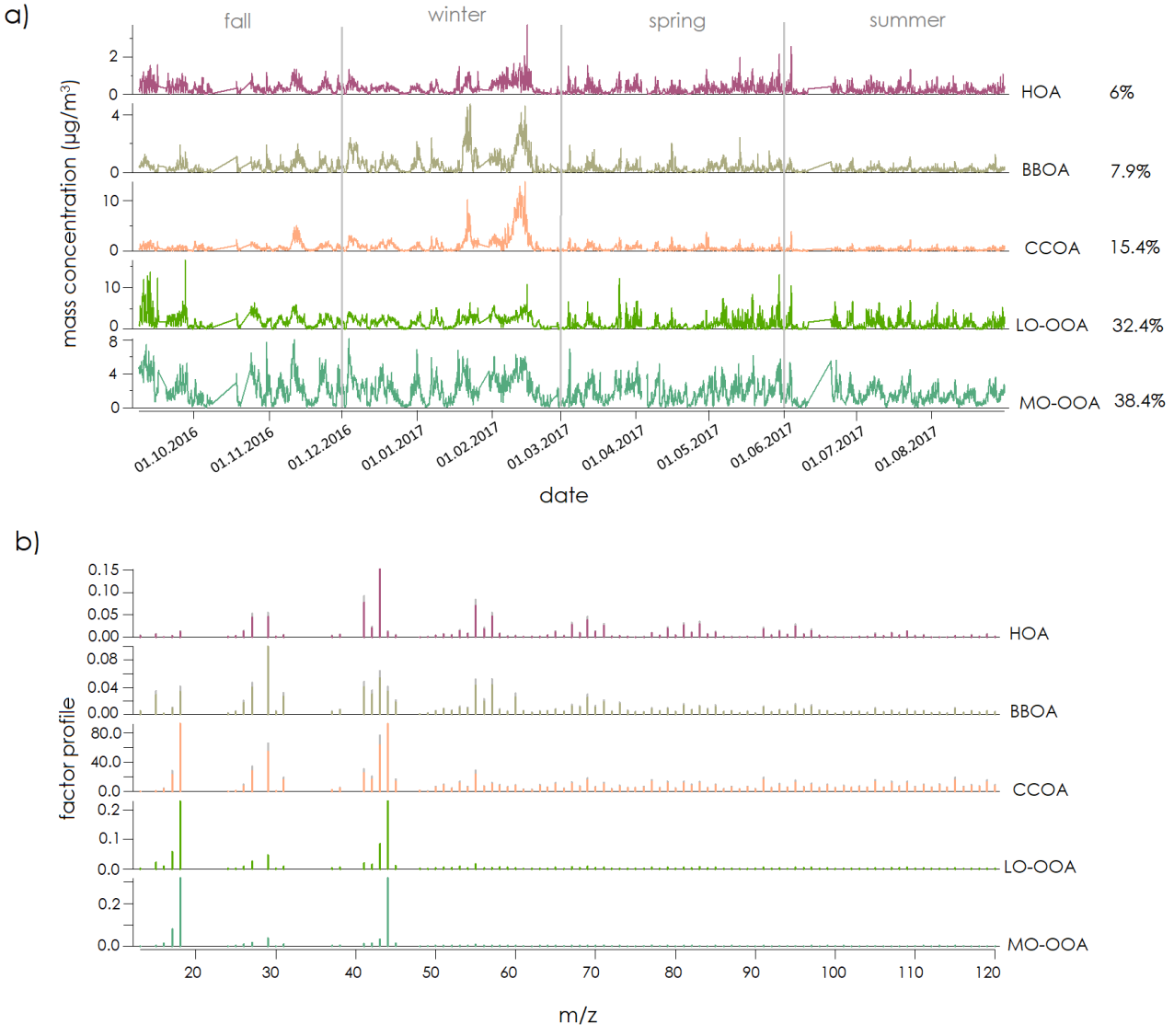

Fig. 4: Overview of averaged PMF (ME-2) results, a) time series, and b) mass spectral profile of organic PMF factors. (Time is in UTC)

https://doi.org/10.5194/acp-2022-842
Preprint. Discussion started: 11 January 2023

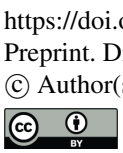

Atmospheric Chemistry and Physics Discussions

1099

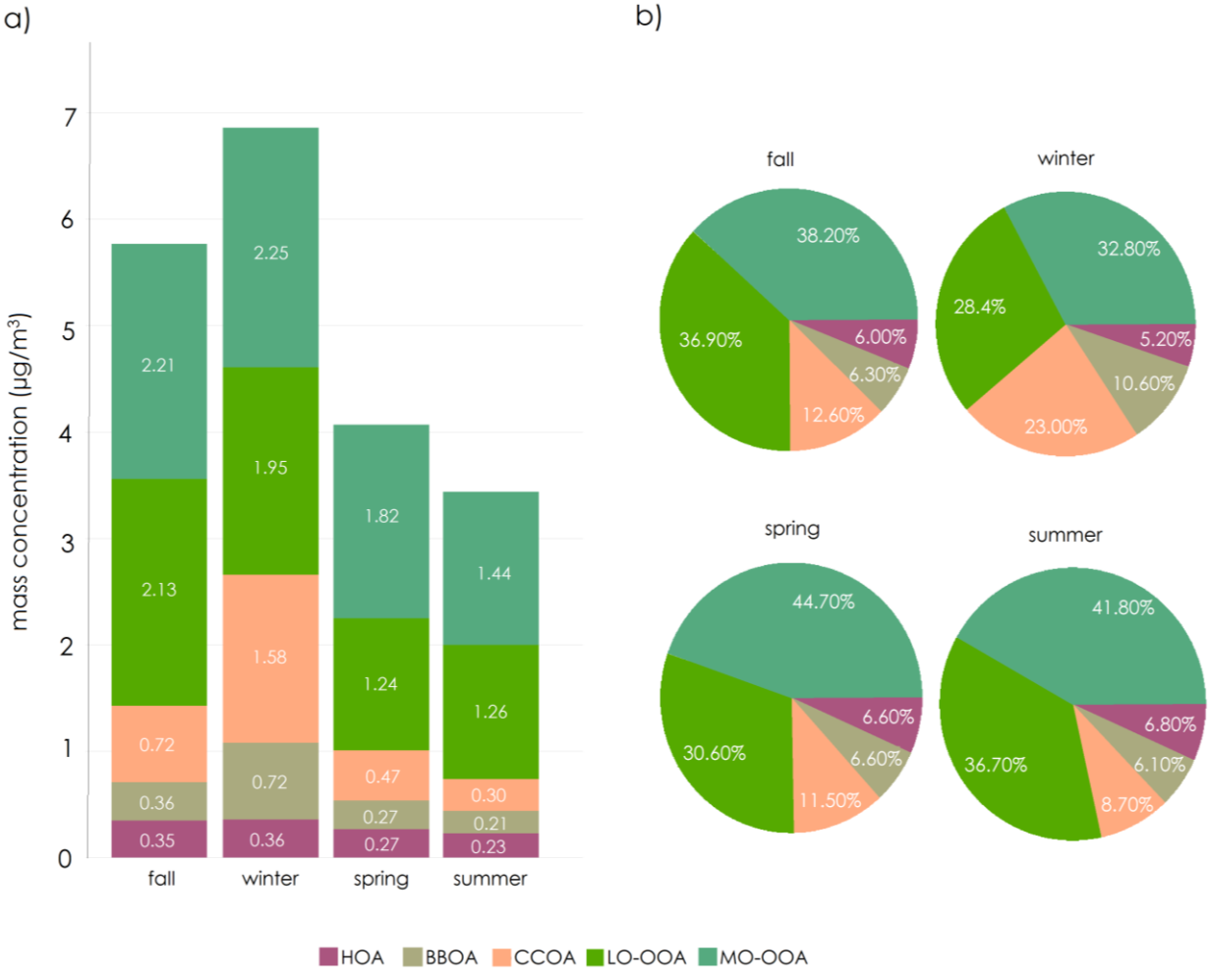

1100

1101 **Fig. 5: Seasonal variation of a) mass concentration, b) mass fraction of PMF source factors.**

https://doi.org/10.5194/acp-2022-842
Preprint. Discussion started: 11 January 2023

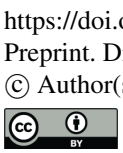

Atmospheric Chemistry and Physics Discussions

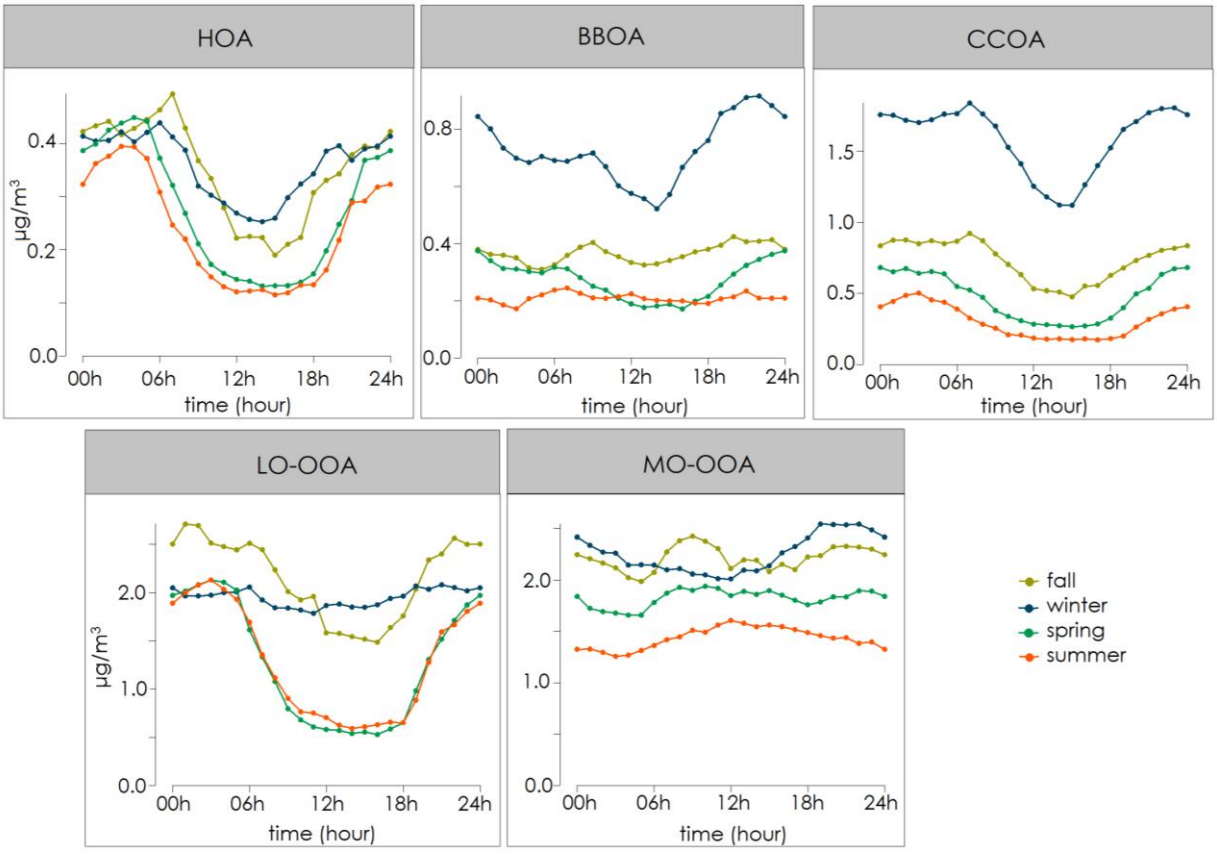

Fig. 6: Seasonal diurnal cycle (hourly averages) of the organic components HOA, BBOA, CCOA, LO-OOA and MO-OOA in UTC time.

https://doi.org/10.5194/acp-2022-842
Preprint. Discussion started: 11 January 2023

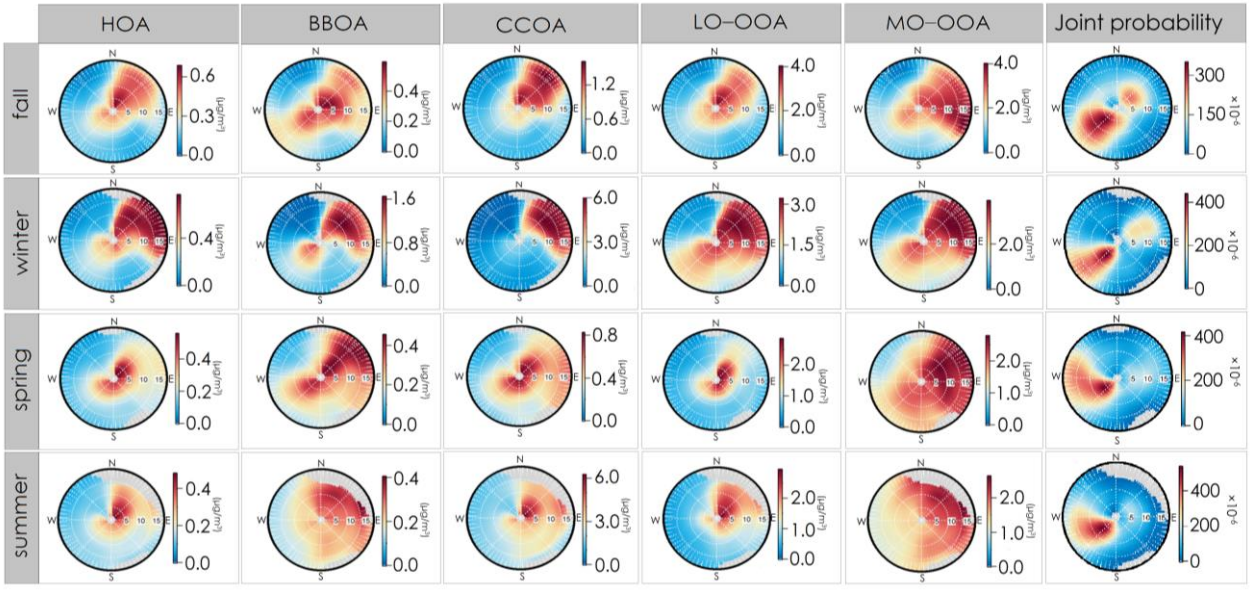

Fig. 7: Seasonal wind roses and NWR plots for the different PMF factors (in µg/m³).

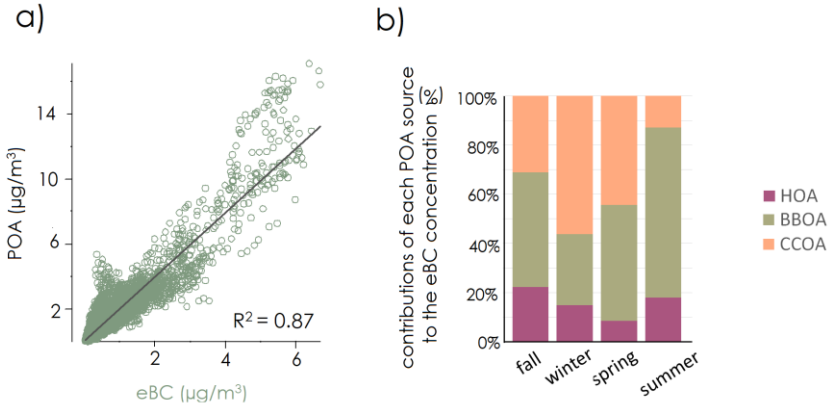

Fig. 8: Contribution of the three POA factors to the mass concentration of eBC, a) scatter plots POA vs eBC and b) contributions of sources to the eBC mass concentration.

https://doi.org/10.5194/acp-2022-842
Preprint. Discussion started: 11 January 2023

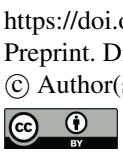

Atmospheric Chemistry and Physics Discussions

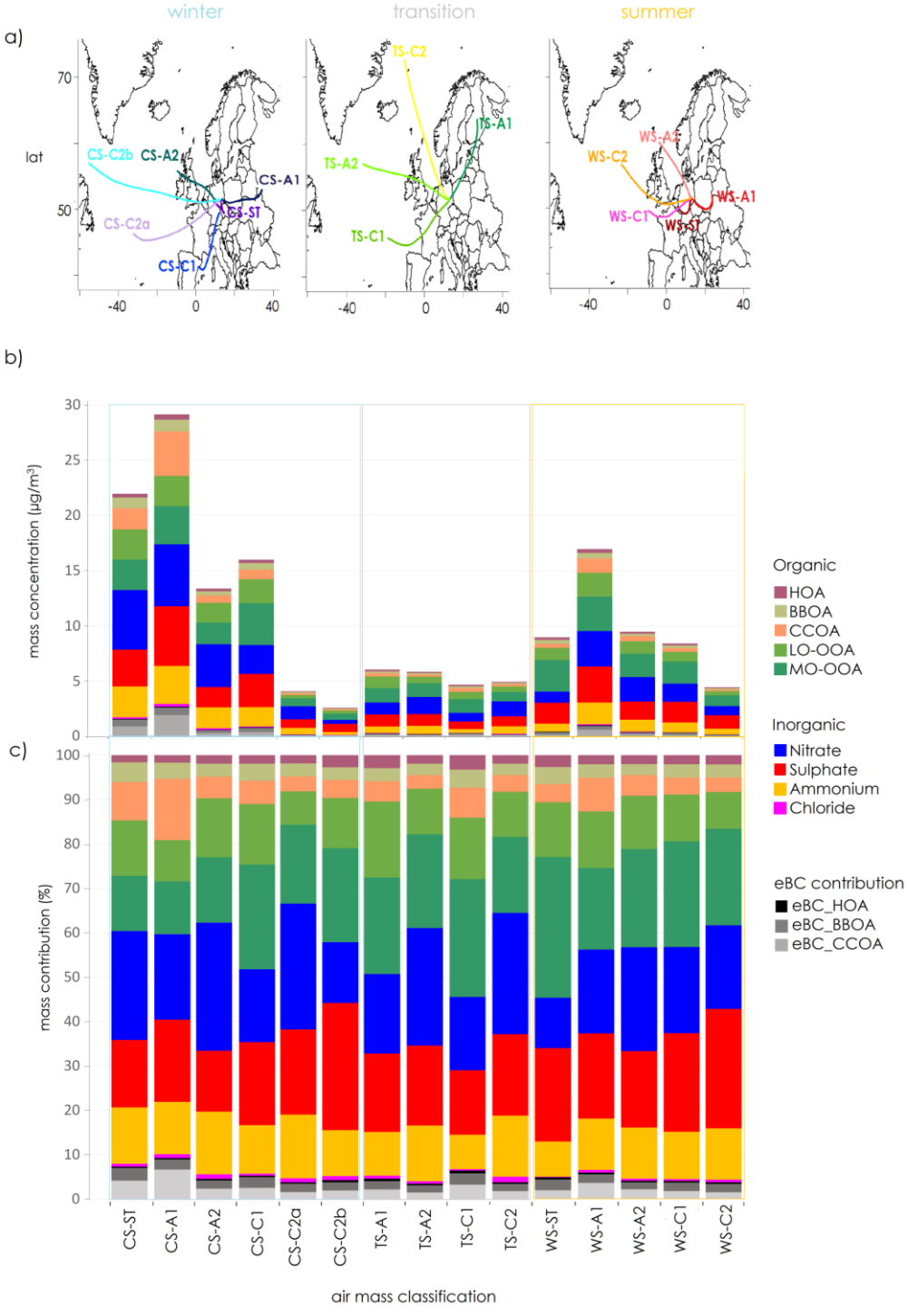

Fig. 9: a) air mass classification based on 13-years backward trajectories cluster analysis at 12:00 UTC, b) influence of air mass to the PM_1 data and PMF factors, and c) contribution of them which averaged from 10:00 to 14:00 UTC.

https://doi.org/10.5194/acp-2022-842
Preprint. Discussion started: 11 January 2023

Atmospheric Chemistry and Physics Discussions

1117

1118 **Table. 2: Main statistical details of the 15 air mass types for total PM_1**

1119 **(CS=Cold Season, WS=Warm Season, ST=Stagnant, A=Anticyclonic, C=Cyclonic).**

Main season	Airmass type	Wind direction	Vorticity	Frequency (%)	Total mean (µg/m^3)
Winter	CS-ST	Stagnating	Anticyclonic	14	21.95
	CS-A1	East	Anticyclonic	18	29.14
	CS-A2	West	Anticyclonic	8	13.39
	CS-C1	South	Cyclonic	10	15.99
	CS-C2a	South West	Cyclonic	3	04.09
	CS-C2b	West	Cyclonic	2	02.60
Transition (Spring/ Fall)	TS-A1	North East	Anticyclonic	4	06.06
	TS-A2	West	Anticyclonic	4	05.86
	TS-C1	South West	Cyclonic	3	04.69
	TS-C2	North West	Cyclonic	4	04.94
Summer	WS-ST	Stagnating	Anticyclonic	6	08.97
	WS-A1	South East	Anticyclonic	11	16.95
	WS-A2	North West	Anticyclonic	6	09.48
	WS-C1	West	Cyclonic	5	08.41
	WS-C2	West	Cyclonic	3	04.46

1120